A tube model for predicting the stress and dielectric relaxations of polydisperse linear polymers �“

Chinmay Das ; Daniel J. Read ✉

Check for updates

CrossMark

View Online

Export Citation

Related Content

Supertubes and Superconducting Membranes

AIP Conference Proceedings (February 2007)

Why, and when, does dynamic tube dilation work for stars?

Journal of Rheology (January 2003)

A constitutive analysis of transient and steady-state elongational viscosities of bidisperse polystyrene blends

Journal of Rheology (January 2008)

A tube model for predicting the stress and dielectric relaxations of polydisperse linear polymers

Chinmay Das[a)] and Daniel J. Read[b)]

School of Mathematics, University of Leeds, Leeds LS2 9JT, United Kingdom

Abstract

We present an algorithm to predict the linear relaxation spectra for linear polymers of fully general and arbitrary polydispersity. As is common in the tube theory descriptions of linear polymers, we assume that the stress relaxation is affected by both the constraint release and tube escape modes, but unlike most existing descriptions we consider how these two modes of relaxation affect each other. We argue that the proper description for relaxation in an arbitrary blend of linear polymers requires consideration of multiple embedded tubes affecting the different relaxation pathways; we propose a novel but minimal description involving five embedded tubes. Building on prior work for binary blends, we derive the scaling level descriptions of the relaxation pathways. We use a large number of existing experimental results on the stress and dielectric relaxations to validate our model, ensuring we explore a very broad range of parameter space. © *2023 Author(s). All article content, except where otherwise noted, is licensed under a Creative Commons Attribution (CC BY) license (http:// creativecommons.org/licenses/by/4.0/).* https://doi.org/10.1122/8.0000605

I. INTRODUCTION

The tube model of de Gennes [1] and Doi and Edwards [2] reduces the complex many-body problem of the relaxation dynamics of polymer melts and concentrated solutions to the relaxation of a test chain in an effective tube-like confining potential [3–5]. Though the tube potential in a melt is due to the chains that relax at the same time scale as the test chain, models that assume a fixed tube diameter yield good agreement with experimental results for the linear viscoelastic responses of monodisperse polymers when contour length fluctuations (CLFs) [6,7] are accounted for.

Since the tube potential in a melt is due to chains that themselves are mobile, the obstacles responsible for the entanglement constraints have a finite lifetime and this leads to constraint release (CR) [8]. Even for monodisperse polymers, CR plays an important role in describing the relaxation process quantitatively. For example, the tube model without CR cannot describe the separation of the dielectric and orientational relaxation time scales for type-A polymers. For monodisperse polymers, satisfactory models based on tube theories that include CR are available, with the model due to Likhtman and McLeish [9] often considered the state-of-the-art.

The effect of CR for polydisperse melts is more pronounced than in the monodisperse case: the original tube model predicts a linear mixing rule [2] for the relaxation function in direct contradiction to experimental findings. Considering entanglements as binary events, Tuminello [10], Tsenoglou [11], and des Cloizeaux [12] incorporated CR in a

simple way in the "double reptation" model to describe polydisperse polymers. The double reptation model and its extensions give a useful tool to describe stress relaxation in polydisperse melt with smooth molar mass distribution, but fails for blends of sufficiently different molar mass species. In particular, it assumes that the relaxation function of a given chain length in a polydisperse melt is unchanged from the relaxation function for the same chain length in a monodisperse melt. This assumption is contradicted by experiments, especially on bidisperse melts where long-chain relaxation is often accelerated upon dilution with short chains [5,13–19].

An alternative approach to the problem is to eschew calculations based on the tube model entirely and to resort to simulations. One such method is the family of slip-link based methods: single chain models such as the discrete slip-link model of Schieber and co-workers [20] and the slip-spring model of Likhtman [21]; or multichain methods such as the NAPLES code [22] or multichain slip-spring models [23]. Although there are differences in detail, these models all include the fundamental processes of reptation, CLF, and CR. Further, once it has been set up and parameterized to function with monodisperse polymers, there is essentially no change in the simulation algorithm required to address polydisperse melts: their relaxation is predicted without further parameter adjustment. Hence, slip-link based models are becoming an efficient and practical method for prediction of rheology of polydisperse linear polymer melts.

It may be tempting, in the light of the success of slip-link models, to claim "job done" and to give the problem no further thought. However, even if a computational model gives perfect predictions, the task remains to describe and quantify the nature of the polymer motion that gives rise to the successful results: how do the processes of CR, CLF, and reptation interact to give the chain dynamics in polydisperse

---

[a)]Electronic mail: C.Das@leeds.ac.uk
[b)]Author to whom correspondence should be addressed; electronic mail: D.J.Read@leeds.ac.uk

melts? As well as being of academic interest, developing this insight provides routes toward yet more efficient calculations, and for improving on algorithms such as the Hierarchical [24], BoB [25], and Time-Marching [26] models for branched polymer relaxation.

A starting point for investigation of chain dynamics of polydisperse melts has been to study the idealized case of a bidisperse melt. Early theoretical work by Doi *et al.* [27] and Viovy *et al.* [28] was based on two competing pictures: Doi *et al.* used a version of the tube dilution model in which long chains were considered to reptate unhindered along tubes diluted by CR from shorter chains; Viovy *et al.* insisted that motion along the diluted tube could only occur at a rate dictated by the frequency of CR events. Both pictures influenced subsequent work, for example, Park and Larson [17,29] followed the tube dilution picture. More recent work by van Ruymbeke *et al.* [19] and Read *et al.* [13,14,30,31] followed more closely the Viovy *et al.* picture (insisting that motion along the diluted tube is at the "rhythm of the release/formation of the short-long entanglements" [19]) but also adding in effects of CLF. Read *et al.* [14,31] also grounded their tube-based theory by comparison to slip-spring simulations.

The model we present below makes extensive use of the results derived in Read *et al.* [13,14,31], generalizing these to include the multiple constraint release (CR) times for fully polydisperse systems. Our approach has been to use this previous work to dictate the overall form of the theoretical model we develop, but also to recognize that most tube-based theory assumes scaling forms that apply best when deep within one dynamical regime or another (e.g., where chains are well entangled, or where constraint release dominates relaxation). In practice, transitions between different dynamical regimes are broad (see e.g., Appendix C of [14]), and almost all experimental results fall close to the transition from one dynamical regime to another: hence we are required to use crossover formulae that interpolate between different dynamical regimes. The transition from entangled to unentangled behavior is particularly troublesome in this regard: the tube model assumes chains have a significant number of entanglements, and so (by design) does not contain the necessary detail to "predict" what happens at the transition. This affects both the early time behavior of the modeling (how to handle motion on time scales close to the entanglement time, τ_e) but also the "disentanglement" that occurs when chains progressively relax by CR. Hence, in developing the model below we have needed to find a path between pragmatism and idealism: using the "ideal" theoretical results to guide the shape of the model, but also pragmatically making use of experimental data to guide choices we have made in handling the many crossovers between regimes. To aid this, we make extensive comparison with experimental results, especially on binary blends, using the two-dimensional projection of parameter space suggested by Doi *et al.* [27] and Viovy *et al.* [28] to ensure we explore the broadest variety of dynamical regimes.

The result, then, is a model that we believe is robust in the sense that it has been tested against a wide range of data and is based upon recent theoretical development. We detail the model in Sec. II and discuss parameterization and comparison to experimental data in Sec. III. We conclude with a summary of the novel developments in our algorithm and with details of how the code can be freely obtained.

II. MODEL

A. Nested tube structure

We begin with a qualitative description of our proposed nested tube structure. Within the tube model for a polymer melt, the relaxation of stress after an instantaneous small step strain is considered to be both due to (i) the chains exiting from the original deformed tube and so able to relax orientation and (ii) and due to CR from relaxation of the chains responsible for the tube constraint. We assume that the relaxation of stress due to CR can be adequately modeled via the dynamic dilution hypothesis [32], which is a coarse-graining operation that connects the effective tube diameter for stress calculation to the fraction of chains already relaxed in a certain time after a step strain. However, we do not follow the subsequent common ansatz of dynamic dilution that chains move freely along this dilated tube subject only to chain friction; rather we account for the extra friction arising from CR events [28]. This is an example of care that is needed during a coarse-graining operation such as dynamic dilution. It is usually clear how to average over fast degrees of freedom when calculating a "static" property such as stress, but the calculation of dynamic quantities such as transport coefficients is harder, because smaller scale dynamics affect the rate of transport at the coarse-grained scale. Our nested tube structure is an attempt to represent these two aspects of the coarse-graining process within the dynamic dilution framework.

The two main modes of motion that allow a polymer to escape from its tube are CLFs of the chain ends [6] and the chain reptation [1,2]. In principle, CR affects both these modes of motion: the chain has some freedom to relax in a wider tube determined by the fraction of unrelaxed polymers. Yet, motion along different tube diameters imposes different friction constants and as a result there are optimal choices of tube diameter for these two relaxation pathways. Figure 1 shows what we consider is a minimal model for describing the relaxation in a system with a wide spectrum of CR time scales. It depicts a number of nested tubes, the meaning of which we now describe.

We begin with three "tube diameters" whose description will be familiar to those who have dealt with previous tube theories based on dynamic dilution. At the time scale τ_e, the entanglement time or the equilibration time, a polymer chain represented by the gray wiggly line is confined in the thin tube of diameter a_0. The thin tube determines the plateau modulus and the early time relaxation. At a later time, the "*fat*" tube diameter a_F is determined by the fraction of chains yet to escape by reptation or CLF from their original tubes; this fat tube is, thus, the largest tube a test chain could possibly explore while confined by its entanglements with currently unrelaxed chains. However, the rate of exploration of the fat tube is limited by friction arising from faster CR events: the thin tube undergoes "CR Rouse motion" but with typically a broad spectrum of CR rates. This CR motion
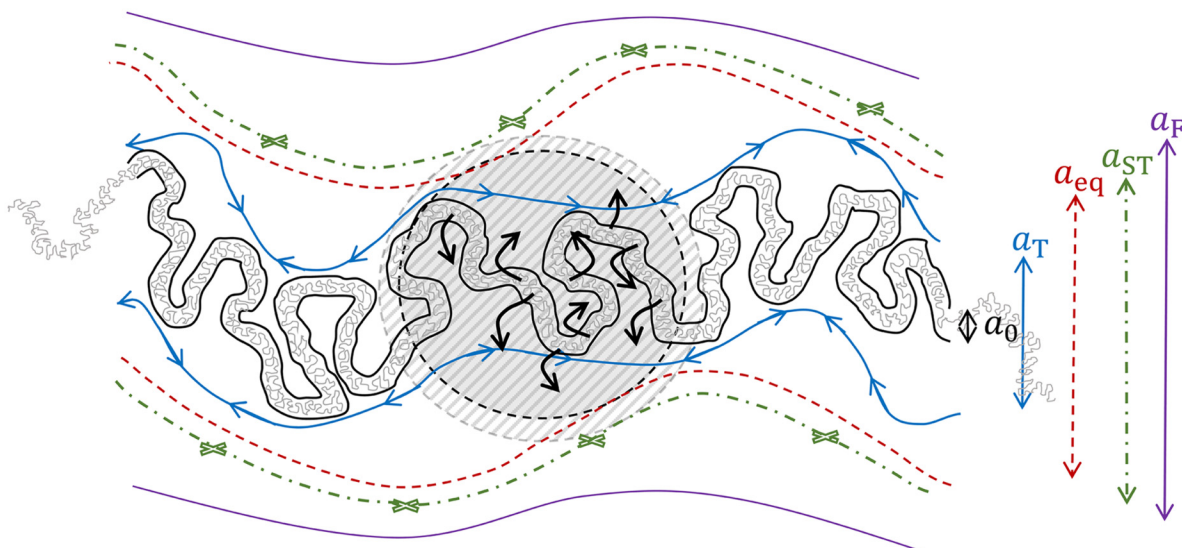
FIG. 1. Multiple embedded tubes required to describe the relaxation of a test chain in an entangled polymer liquid.

allows the chain to relax stress coming from chain subsections up to a "supertube" diameter $a_{ST} \leq a_F$, depicted in Fig. 1 by the arrows indicating hops of the thin tube. So, in previous works on tube theory, a_{ST} determines stress relaxation from CR. For a sufficiently broad spectrum of CR times, the fat tube diameter increases slowly and $a_{ST} = a_F$. However, if a large fraction of the polymers escape their tubes at similar times, then a_F increases sharply, but the rate of increase of a_{ST} is limited to a power law commensurate with CR Rouse motion, until it "catches up" with a_F. These three "tube diameters" have been commonly used in many publications on tube theory, see, e.g., [5,24,25,33,34]. We retain this broad picture, but with some modifications to the details as indicated below.

We now introduce two further "tube diameters," also depicted in Fig. 1, which we consider are necessary for a full description. As noted above, chain motion along tubes of different diameters is subject to different friction. At the smallest scale, motion along the thin tube a_0 is subject only to the chain friction. Motion directly along the primitive path of any larger tube diameter is only possible via CR events, and so is subject to the friction arising from these CR events. Typically, exploration of wider tubes requires slower CR events, and so is subject to greater friction. On the other hand, the primitive path of wider tubes is smoother and shorter: a chain does not need to travel so far along a wider tube to achieve the same overall (3D) displacement. There is, thus, a competition between motion along thinner tubes (lower friction but a more tortuous path) and wider tubes (higher friction but smoother path). In principle, motion along all tube diameters occurs simultaneously, but we simplify the picture by seeking the optimal tube for chain transport "along" the nested tube structure. This optimal tube determines the fastest route for reptation and is shown in Fig. 1 as the tube with arrows along the tube contour, with tube diameter a_T.

We finally define an "equilibration" tube diameter, a_{eq}. In past works on binary blends, consideration of CLFs has

noted the requirement to make a distinction between (i) the tube diameter for the fastest chain transport along the tube detailed above and (ii) the tube diameter within which the chain has freedom to retract. The latter requires only a *local* equilibration in the tube, while the former involves a large-scale chain transport from one section of tube to another. The physical picture is that local rearrangements of the tube structure give rise to local fluctuations in tube length, giving the necessary freedom for CLF; these then couple to chain transport along the tube, giving rise to the actual CLF. For example, in many binary blends, chain transport is fastest along the thin tube, yet CR events permit local equilibration in the fat tube, and so "fat tube" CLF (i.e., to a depth permitted by fat tube constraints) is achieved in practice via chain transport along the thin tube [13,14,31]. It should be clear from the above that the tube diameter a_T determines the optimal mode for chain transport along the tube for CLF (as well as for reptation). Yet, we still need to consider which tube diameter gives freedom for *local* equilibration, specifically for CLF. A first (and good) guess would be the supertube diameter a_{ST} within which local stress relaxation occurs. We note, however, that the equilibration process we are discussing is distinct from the orientation relaxation required for stress relaxation and potentially requires a greater number of CR events to achieve. So, while obviously being related to the same CR events, it may have slower dynamics. We, thus, propose a further tube diameter a_{eq}, defined as the tube diameter within which CLF has freedom to occur at any given time scale. Evolution of a_{eq} with time is naturally driven by the same events as for a_{ST} and so (as will be apparent below) our suggested dynamics for the two are closely related. Our (very much pragmatic) reasons for distinguishing the "supertube" from the "equilibration tube" are that (i) they are not *a priori* obviously the same, (ii) comparison of our theory with a wide range of experimental data suggested a need to distinguish them, and (iii) we realized that previous work examining the theoretical description of CLF in slip-spring simulations with CR also made use of two different tube

diameters in this way, even though it was not noted or explicitly discussed [14]. In Appendix A, we outline the main results from those slip-spring simulations that indicate the need for a separate "supertube" and "equilibration tube." We also indicate how making this distinction affects our predictions in practice. Because of the closely related nature of a_{eq} and a_{ST}, in Fig. 1, we depict the exploration volume for the equilibration tube with a dark gray circle and the supertube with a lighter gray circle.

Finally, we note that each of the tube diameters a_I described above (where I could be fat tube, supertube, etc.) may be related to an associated level of dilution ϕ_I via an equation of form $a_I = a_0 \phi_I^{-\alpha/2}$, where α is the dilution exponent, e.g., a_{ST} and ϕ_{ST} are related via

$$a_{ST}(t) = a_0 \phi_{ST}^{-\alpha/2}(t). \tag{1}$$

Having now qualitatively described our proposed nested tube structure, we now proceed to the technical details of how to track these various tube diameters within a computational algorithm, and how we use them to obtain the relaxation modes of the chains. A reader not interested in these technical details could proceed to the results in Sec. III.

B. Stress relaxation and tube escape

We assume that the stress relaxation modulus $G(t)$ can be expressed as a product of a term $\mu(t)$ characterizing the tube survival probability and a term $R(t)$ characterizing the CR contribution as

$$G(t) = G_N^0 \, \mu(t) R(t), \tag{2}$$

with G_N^0 being the plateau modulus. For a multicomponent melt, direct determination of $\mu(t)$ and $R(t)$ is difficult. Instead, in a manner similar to previous works on branched polymers [24–26], for each polymer component i we track the amount of chain end escaped from the original tube, $z_i(t)$ (counted in units of thin tube entanglements). We then express the fraction of material still confined in the deformed tubes as

$$\phi(t) = \sum_i w_i \left(1 - \frac{2z_i(t)}{\mathcal{Z}_i}\right). \tag{3}$$

Here, w_i is the weight fraction of the ith component with a total number of entanglement $\mathcal{Z}_i$, and the sum is over all the different components. Our computational scheme is made self-consistent by computing the relaxation dynamics of individual chains $z_i(t)$ based on the mean field $\phi(t)$, which is determined itself from Eq. (3).

We assume that the reduction of the tube survival probability $\mu(t)$ from a change in ϕ at time $t = \tau$ is not instantaneous, but has an exponential distribution about τ, and can be expressed as

$$\mu(t) = -\int_0^\infty \frac{d\phi}{d\tau} e^{-t/\tau} d\tau. \tag{4}$$

The above transformation from $\phi(t)$ to $\mu(t)$ is a computational and calculational convenience similar to that used in the BoB and Hierarchical models [24,25]. It can be considered analogous to the "box diagrams" used as a cartoon for stress relaxation processes in, e.g., [5,27,28]. In the "box diagram," a single exponential relaxation with time constant τ is represented as a sharp, instantaneous drop in $\phi(t)$ at $t = \tau$. Hence, the derivative $-(d\phi/dt)$ of the box diagram gives the relaxation spectrum (and has a δ-function at $t = \tau$ for single exponential relaxation). Equation (4) then converts from the box diagram $\phi(t)$ to $\mu(t)$. Computationally, this assumption leads to the simplification that reptation can be considered a single time event in relaxation of $\phi(t)$, while retrieving the proper reptation spectrum in the final calculation for the relaxation moduli via $\mu(t)$. It should be noted that in this formalism $\mu(t)$ is the true tube survival probability (reaching zero only asymptotically at infinite time) while $\phi(t)$ is merely a calculational tool toward $\mu(t)$ [$\phi(t)$ can become zero at finite time when one might say "everything has relaxed"].

When predicting dielectric relaxation of polyisoprene below, we assume that the dielectric relaxation is proportional to $\mu(t)$. This is appropriate for samples in which the dipoles have a component pointing along the chain in a single direction, but not in cases where the dipole direction inverts along the chain [35,36]. In the latter case, a more detailed formulation would be required. Also, our assumption of dielectric responses being proportional to $\mu(t)$ neglects additional contributions to the dielectric relaxation from fluctuations of the chain about the tube axis at the ends [37]. For this reason, when comparing with the dielectric loss measurement ϵ'', we mark our predictions as μ'' to highlight that these two quantities are not exactly the same. When chains are only a few entanglements long, this difference can be significant.

In a similar manner, we obtain the CR term $R(t)$ from the "supertube fraction" ϕ_{ST} [see Eq. (1)] as

$$R(t) = -\int_0^\infty \frac{d\phi_{ST}^\alpha}{d\tau} e^{-t/\tau} d\tau. \tag{5}$$

We detail later how ϕ_{ST} is obtained within our computational scheme. As in the calculation of $\mu(t)$, the exponential distribution in the calculation of $R(t)$ allows for a simple accounting of multiple CR events in a blend. The Maxwell forms of $\mu(t)$ and $R(t)$ also enable us to sample discrete time relaxation in logarithmically spaced time intervals without introducing spurious high-frequency oscillations in the dynamic moduli.

Readers familiar with previous works on prediction of branched polymer rheology [5,24,25,33,34,38] may note that the above scheme for calculating stress relaxation differs from those earlier works. The formula for stress relaxation proposed by Milner and co-workers [33,34,38] and used in later computational schemes (including by us) [24,25] was

$$G(t) = -G_N^0 \int_0^\infty \frac{d(\phi \phi_{ST}^\alpha)}{d\tau} e^{-t/\tau} d\tau. \tag{6}$$

Our reason for setting Eq. (6) aside in the current work is (as

detailed in Appendix B) that it is inconsistent with double reptation for binary blends, resulting in the impossibility of successful simultaneous prediction of dielectric and stress relaxation data. Similar criticisms of Eq. (6) were made previously by Shchetnikava *et al.* [39] and the analysis in Appendix B resolves their substantive point, which is a factor of two error in the terminal time. We note that using Eq. (2) in place of Eq. (6) is certainly not novel: Eq. (2) is used in Likhtman and McLeish's (LM) theory for monodisperse linear polymers [9] and in Watanabe's analysis of dynamic tube dilation using rheology and dielectric spectroscopy [36].

In the rest of this section, we develop scaling level arguments for the relaxation of $z(t)$ and $\phi_{ST}(t)$.

C. CR and the evolution of the supertube fraction

As common with existing theories [5,9,13,14,28,31,33,34], we model CR as a Rouse relaxation process. Before formulating a theory for a broad spectrum of CR time scales, we consider first the highly idealized case of a single, slow, CR time scale of $\tau_{CR} \gg \tau_e$. The effective friction per monomer from the CR hops is determined by the time scale τ_{CR} and is expressed as

$$\frac{\zeta_{CR}}{\zeta_0} = A_\zeta \frac{\tau_{CR}}{\tau_e}, \qquad (7)$$

where ζ_0 is the bare monomer friction and A_ζ is a scaling parameter found to be substantially smaller than 1 in slip-spring simulations [31]. In general, both bare monomer friction and CR friction contribute to relaxation behavior and we denote the total friction as $\zeta_{tot} \equiv \zeta_{CR} + \zeta_0$. For long chains, the behavior of $R(t)$ at intermediate times (much longer than τ_{CR} but shorter than the terminal relaxation time) can be deduced from the stress relaxation of the usual Rouse model by replacing the monomer friction with ζ_{tot} as

$$\phi_{ST}^\alpha(t) \simeq R(t) = \sqrt{\frac{\pi}{8}} \sqrt{\frac{\zeta_{tot}}{\zeta_0} \frac{\tau_e}{t}}$$
$$= \sqrt{\frac{\pi}{8} A_\zeta} \sqrt{1 + \frac{1}{A_\zeta} \frac{\tau_e}{\tau_{CR}}} \sqrt{\frac{\tau_{CR}}{t}}, \qquad (8)$$

where the prefactor $\sqrt{\pi/8}$ comes from the relaxation modulus $G(t)$ from solution of the standard Rouse model.

Concentrating on the limiting case of $\tau_{CR} \gg \tau_e$ such that the monomer friction can be ignored, extrapolating this long-time power-law form of ϕ_{ST} back to time $t = \tau_{CR}$ yields

$$\phi_{ST}(\tau_{CR}) \simeq \left[\frac{\pi}{8} A_\zeta\right]^{\frac{1}{2\alpha}} \equiv 1 - \delta_{CR}^\infty, \qquad (9)$$

whereas, for $t < \tau_{CR}$, no relaxation by CR has occurred and $\phi_{ST} = 1$. Comparing these two suggests that ϕ_{ST} should remain equal to 1 for $t < \tau_{CR}$, then drop by a fraction δ_{CR}^∞ at $t = \tau_{CR}$, before relaxing via the power-law Eq. (8) for $t > \tau_{CR}$. Substitution into Eq. (5) yields, for $R(t)$, an exponential relaxation with time scale $t = \tau_{CR}$ followed by long-

time power-law decay. The physical basis for this is that CR events involve substantial local changes in tube configuration: they are finite-sized hops of order the tube diameter occurring at time scale τ_{CR}. Hence, a substantial relaxation occurs at τ_{CR}, followed by the power-law relaxation from the summed effect of multiple tube hops over much larger lengthscales. This is in contrast to the standard Rouse model (for a chain, rather than a tube) in which the stochastic diffusive bead motion is continuous, involving infinitesimal hops rather than finite hops. So, for tube motion at time scale τ_{CR}, it is not appropriate to immediately apply the power-law decay based on the Rouse model; rather, there should be a drop in ϕ_{ST} at τ_{CR} followed by a power-law decay.

We note that the above result is different from the standard assumption in several existing models about the supertube relaxation (e.g., our own [25]) in which ϕ_{ST} undergoes power-law decay from initial value $\phi_{ST} = 1$ at $t = \tau_{CR}$ (i.e., without the drop by δ_{CR}). In the present work, we have found that this drop, combined with the formulation of $G(t)$ in Eq. (2), is crucial in reconciling the differences in the relaxation time scales observed in the rheological and dielectric responses of monodisperse melts and binary blends.

The above applies when $\tau_{CR} \gg \tau_e$. As τ_{CR} approaches τ_e, the monomer friction becomes significant compared to friction from CR hops and reduces the rate of diffusion from CR events. As a result, ϕ_{ST} does not drop so strongly at $t = \tau_{CR}$ before attaining the power-law Rouse relaxation. We account for this by making the "drop" δ_{CR} dependent on τ_{CR} as

$$\delta_{CR}(\tau_{CR}) = 1 - \left[1 - \delta_{CR}^\infty\right] \sqrt{1 + K_\zeta \frac{\tau_e}{\tau_{CR}}} \qquad (10)$$

where the form of the last term is inspired by the balance of CR and monomer friction in Eq. (8). Since the tube picture emerges only for $t \simeq \tau_e$, we assume $\phi_{ST} = 1$ for $t < \tau_e$. To have the correct response from solvent, we enforce $\delta_{CR}(\tau_{CR} = \tau_e) = 0$ in Eq. (10) which fixes K_ζ in terms of the parameter δ_{CR}^∞ to be

$$K_\zeta = \frac{1}{\left(1 - \delta_{CR}^\infty\right)^2} - 1. \qquad (11)$$

We now consider a generic polymer melt, in which there will typically be a spectrum of constraint release time scales. Our strategy is to treat the unrelaxed fraction $\phi(t)$ as the primary dynamical variable, which decreases as chains escape their tube by reptation and contour length fluctuation. But, such tube escape also gives rise to CR, so the variation of $\phi(t)$ also encodes the spectrum of CR times: we need to determine how the decrease of $\phi(t)$ gives rise to the variation of $\phi_{ST}(t)$. A slow decrease in $\phi(t)$ indicates a sufficiently broad distribution of CR time scales (to be quantified below) so that we can assume that the double reptation picture holds and $\phi_{ST}(t) = \phi(t)$. Yet, a more rapid decrease in $\phi(t)$ (e.g., when many chains reptate at the same time) indicates a substantial amount of CR occurring at a single time scale and this causes an entry into a "supertube relaxation" regime with

quasi-power law decay of $\phi_{ST}(t)$ subject to constraint $\phi_{ST}(t) \geq \phi(t)$.

We work within a discrete time stepping scheme, in which $\phi(t)$ decreases by $\Delta\phi$ during time step Δt. As will be explained in Secs. III E and III F, the value of $\Delta\phi$ is deduced from the effects of CLF and reptation on Eq. (3). For now, let us assume that $\Delta\phi$ is known and examine the consequent effect on ϕ_{ST}. Consider a certain time t^* at which this change $\Delta\phi$ takes place during the next step. We denote the value of ϕ_{ST} immediately preceding t^* as ϕ_{ST}^*. In Eq. (9), where *all* constraints relaxed at the same time, the drop in ϕ_{ST} was δ_{CR}^∞. If only a fraction of $\Delta\phi$ constraints are removed, then ϕ_{ST} would be immediately reduced by $\delta_{CR}^\infty\Delta\phi$ (i.e., in proportion to the number of constraints removed). This applies if $t^* \gg \tau_e$; for general t^*, we instead use δ_{CR} as obtained from Eq. (10) evaluated at $\tau_{CR} = t^*$. Following the drop in ϕ_{ST}, there follows a power-law decay according to Rouse scaling so that at the end of the time step,

$$\phi_{ST}^\alpha(t^* + \Delta t) = [\phi_{ST}^* - \delta_{CR}\Delta\phi]^\alpha \sqrt{\frac{t^*}{t^* + \Delta t}}. \quad (12)$$

We then enforce the constraint $\phi_{ST}(t) \geq \phi(t)$. If the value of $\phi_{ST}(t^* + \Delta t)$ resulting from Eq. (12) is less than $\phi(t^* + \Delta t) = \phi(t^*) - \Delta\phi$, then we enforce $\phi_{ST}(t^* + \Delta t) = \phi(t^* + \Delta t)$, i.e., the relaxation is not in the "supertube relaxation" regime and $\phi_{ST}(t) = \phi(t)$. On the other hand, if $\phi_{ST}(t^* + \Delta t)$ is greater than $\phi(t^* + \Delta t)$ then we move to the next time step without adjusting ϕ_{ST}: here, we are in the supertube regime and $\phi_{ST}(t) > \phi(t)$. A sketch of the variation in ϕ_{ST} during a single time step is shown in Fig. 2, indicating the two possible scenarios. For the solid green line, $\phi_{ST}(t) > \phi(t)$ at the end of the time step and the simulation remains in the supertube regime; for the dashed red line, $\phi_{ST}(t) = \phi(t)$ is enforced at the end of the time step. Note that the initial drop in ϕ_{ST} can never take ϕ_{ST} below $\phi(t^* + \Delta t)$ because ϕ_{ST} is always greater than or equal to ϕ at the start of the time step, and the initial drop in ϕ_{ST} is always less than the drop in ϕ (i.e. $\delta_{CR} < 1$ for all τ_{CR}).

Now we can quantify what counts as sufficiently slow decrease of $\phi(t)$ to avoid entering the "supertube" regime. Considering a discrete time interval Δt, a supertube relaxation regime is initiated if

$$\Delta\phi > \phi_{ST}^* \frac{1 - \left(\frac{t^*}{t^* + \Delta t}\right)^{1/2\alpha}}{1 - \delta_{CR}\left(\frac{t^*}{t^* + \Delta t}\right)^{1/2\alpha}}. \quad (13)$$

We note that Eq. (12) is applied even within the supertube relaxation regime. Thus, if further reductions of ϕ occur during supertube relaxation, by an amount $\Delta\phi$ during time step Δt, then the instantaneous reduction of ϕ_{ST} by $\delta_{CR}\Delta\phi$ is still applied. Hence, in this scheme, supertube relaxation is not a pure power-law decay, because it continues to be affected by further reductions in ϕ. This is necessary so that the relaxation predicted by drops of $\Delta\phi_1$ and $\Delta\phi_2$ over two subsequent time steps is practically equivalent to that from a drop of $\Delta\phi_1 + \Delta\phi_2$ all applied over a single time step (i.e., so that the scheme is insensitive to the chosen discretization of time). It can also be argued on physical grounds: extra CR events still produce extra hops in tube configuration even in the supertube regime.

The above indicates how $\phi_{ST}(t)$ may be obtained from $\phi(t)$ within an algorithm based on a discrete time step. To complete the algorithm, we need to compute $\phi(t)$ arising from chain reptation and CLF. For this, we note that $\phi_{ST}(t)$ (or $a_{ST}(t)$) encodes how far a chain trapped in a tube can move via CR, i.e., it indicates the effective friction for CR events acting at different lengthscales, which is required for prediction of reptation and CLF along tubes of different diameters.

For chain motion along a tube with diameter a_{ST} (determined from ϕ_{ST}), we associate an effective friction constant per monomer by inverting the first equality in Eq. (8), giving

$$\left(\frac{\zeta_{tot}}{\zeta_0}\right)_{|a_{ST}} = B_\zeta \frac{t(\phi_{ST})}{\tau_e} \phi_{ST}^{2\alpha}. \quad (14)$$

Here, $t(\phi_{ST})$ is the time at which $\phi_{ST}(t)$ reaches a given value corresponding to diameter a_{ST} via Eq. (1). We have introduced an order one constant B_ζ. If $\phi_{ST}^\alpha(t)$ were to behave identically as $R(t)$, $B_\zeta \simeq (8/\pi)$—but in practice $\phi_{ST}^\alpha(t)$ and $R(t)$ are not identical and we fixed B_ζ at a value close to $8/\pi$ that gave good predictions across a wide range of data. Note that the friction obtained from Eq. (14) is valid only for $t \gg \tau_e$ and we assume that $\phi_{ST}(t) = 1$ for $t \leq \tau_e$ (i.e., the supertube diameter remains identical to the thin tube diameter for $t \leq \tau_e$).

As time t increases [as does $a_{ST}(t)$], $\phi_{ST}(t)$ decreases. Then, Eq. (14) allows us to evaluate the effective friction for motion along tubes at each diameter. So, Eq. (14) is evaluated at each time, t, yielding the effective friction per monomer for motion along tubes with diameter $a_{ST}(t)$. This information is then used to determine the subsequent relaxation dynamics of the chains, from which we update $\phi(t)$. Given the update of $\phi(t)$, we then update $\phi_{ST}(t)$ as indicated
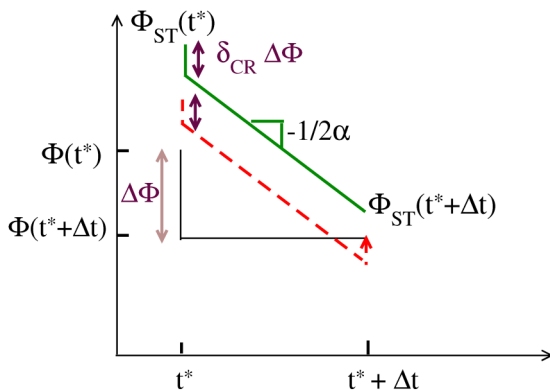

FIG. 2. Schematic representation of the change in ϕ_{ST} in a single time step. Both the axes are in logarithmic scale. Two scenarios are indicated. For the solid green line $\phi_{ST}(t) > \phi(t)$ at the end of the time step and the simulation remains in the supertube regime; for the dashed red line $\phi_{ST}(t) = \phi(t)$ is enforced at the end of the time step.

above; these steps form a self-consistent iterative loop to update all variables at each increment of time.

D. "Equilibration" tube diameter

As noted in Sec. II A, we define an "equilibration" tube diameter, a_{eq}, which is the largest tube diameter within which CLFs can be considered, and sets a maximum accessible tube for reptation to be considered. We argue that it takes a number of CR hops up to a given lengthscale before the tube is sufficiently equilibrated at that scale such that translational motion along that tube diameter can occur. Again, we consider the long-time situation first, in which $t \gg \tau_e$. Eq. (14) gives the effective total friction per monomer at the scale of a tube diameter a_{ST}. We can define a Rouse "equilibration time" by scaling up from the bare entanglement time τ_e to the scale of a_{ST}, accounting for the extra effective friction,

$$\tau_{e,a_{ST}} = \tau_e \left(\frac{\zeta_{tot}}{\zeta_0}\right)_{|a_{ST}} \phi_{ST}^{-2\alpha}. \tag{15}$$

Using Eq. (14) gives

$$\tau_{e,a_{ST}} = B_\zeta t(\phi_{ST}). \tag{16}$$

This simply serves to illustrate that although local equilibration and stress relaxation are linked, it would be a mistake simply to define equilibration time from dynamics of ϕ_{ST} without further consideration. With $B_\zeta \simeq 8/\pi$, it suggests "equilibration" at scale a_{ST} is delayed as compared to the stress relaxation.

The scaling level description, especially the expression for the friction coefficient in Eq. (8), holds only for $t \gg \tau_e$. Simulations with slip-spring models show that fast CR ($\tau_{CR} \sim \tau_e$) introduces significantly larger friction for diffusion than the linear form in Eq. (8) would predict [31]. We heuristically account for these by allowing ϕ_{ST} to relax only for $t \geq \tau_e$ and using a modified expression for the equilibration time as

$$\tau_{e,a_{ST}} = A_{eq} t(\phi_{ST}) \left(1 + B_{eq}\sqrt{\frac{\tau_e}{t(\phi_{ST})}}\right). \tag{17}$$

Here, $A_{eq} \simeq B_\zeta$, and the new parameter B_{eq} further delays equilibration at short times and forces CLF in the thin tube at short times. The particular form in Eq. (17) is motivated by the expression of CR friction from slip-spring simulations [31] and physically accounts for the influence of the chain friction on hop lengths.

Consider a particular time, t^*: we first obtain $\phi_{ST}(t^*)$ as detailed above in Sec. II C, i.e., $t(\phi_{ST}) = t^*$. We then use Eq. (17) to determine the equilibration time $\tau_{e,a_{ST}}$ for that level of dilution. Hence, the time at which ϕ_{eq} will (later) become equal to $\phi_{ST}(t^*)$ is $\tau_{e,a_{ST}}$, i.e., $\phi_{eq}(t = \tau_{e,a_{ST}}) = \phi_{ST}(t^*)$. Noting that $\tau_{e,a_{ST}} > t^*$, this process allows us to predict, and store, the evolution of $\phi_{eq}(t)$ into the immediate future beyond current time t^*.

Now, at current time t^*, we also need the *current* value of $\phi_{eq}(t = t^*)$, which is required to determine the subsequent evolution of $\phi(t)$ as detailed below. But since $\phi_{eq}(t)$ has been stored from previous time steps, we are always able to determine $\phi_{eq}(t^*)$ by interpolation between the previously stored data.

E. Reptation

Diffusion along fatter tubes requires a larger friction constant (due to longer CR times) but involves motion over shorter contour lengths. The competition between these determines the optimal tube diameter that is most advantageous for reptation. We assume that motion along a single tube diameter, $a_T(t)$, contributes overwhelmingly in the reptation relaxation at time t. To determine $a_T(t)$, we calculate the reptation time in all accessible tubes, i.e., tubes with $a \leq a_{eq}(t)$, and select the one with the lowest predicted reptation time.

To estimate the friction coefficient appropriate for motion along tube of diameter a_{ST}, we calculate the CR contribution to the friction from Eq. (14) as $\zeta_{tot} - \zeta_0 = \zeta_0(B_\zeta(t/\tau_e)\phi_{ST}^{2\alpha} - 1)$. This CR allows motion directly along the tube at diameter a_{ST}. We additionally include the contribution of free diffusion along the bare tube (of diameter a_0) projected onto the scale a_{ST} (such free diffusion always occurs, even in the absence of CR). To calculate the sum of free diffusion along thin tube and CR diffusion along tube of diameter a_{ST}, we follow Read *et al.* [13] using their form for the friction coefficient for translational diffusion as

$$\left(\frac{\zeta_T}{\zeta_0}\right)_{|a_{ST}} = \frac{1}{\phi_{ST}^\alpha + 1/\left[B_\zeta \frac{t(\phi_{ST})}{\tau_e} \phi_{ST}^{2\alpha} - 1 + \frac{1}{1 - \phi_{ST}^\alpha}\right]}. \tag{18}$$

Then, the time scale of reptation in a_{ST} at some time $t \geq \tau_{e,a_{ST}}$ is given by

$$\tau_{d,a_{ST}}(t) = \frac{N\zeta_T}{\pi^2 k_B T} \left\{\phi_{ST}^\alpha (\mathcal{Z} - 2z(t))^2 a_0^2\right\}$$

$$= 3\mathcal{Z}(\mathcal{Z} - 2z(t))^2 \tau_e \phi_{ST}^\alpha \left(\frac{\zeta_T}{\zeta_0}\right)_{|a_{ST}}$$

$$\equiv \tau_{d,a_0} \Psi(a_{ST}). \tag{19}$$

Here, we have included the reduction in the diffusion length from CLFs achieved in time t, and $\tau_{d,a_0} \equiv 3\mathcal{Z}(\mathcal{Z} - 2z(t))^2 \tau_e$ refers to the reptation time in the thin tube with the same reduction in the diffusion length from CLF. The factor

$$\Psi(a_{ST}) = \phi_{ST}^\alpha \left(\frac{\zeta_T}{\zeta_0}\right)_{|a_{ST}} \tag{20}$$

gives the amount by which reptation enhanced by CR along some tube a_{ST} is faster than purely along the thin tube. The factor ϕ_{ST}^α in Eq. (20) arises from a geometric factor corresponding to decreased primitive path contour length for motion along the diluted tube. The factor $(\zeta_T/\zeta_0)_{|a_{ST}}$ corresponds to the increase in friction required to move along that

tube by CR motion. These two factors are frequently in competition: the first always speeds up the reptation time, while the latter slows it down.

To find the optimal tube for reptation at some time t, we consider reptation along all tubes of diameter $a_{ST} < a_{eq}(t)$ (noting that the time $t_1 = t(\phi_{ST})$ at which the supertube diameter reached a_{ST} is certainly earlier than t). The minimum of $\Psi(a_{ST})$ over $a_0 < a_{ST} < a_{eq}(t)$ is denoted as $\Psi_{min}(t)$, and this determines the tube diameter with the shortest reptation time, i.e., the optimal reptation time at time t is

$$\tau_d(t) = \tau_{d,a_0}\Psi_{min}(t). \tag{21}$$

We denote the tube diameter associated with the minimum of $\Psi(a_{ST})$ as a_T, with corresponding dilution ϕ_T.

We note that, perhaps surprisingly, the above analysis shows that (i) the factor $\Psi(a_{ST})$ in Eq. (20), (ii) its minimum value $\Psi_{min}(t)$ at a given time, and consequently also (iii) a_T at a given time *take the same value for all chains independent of molecular weight!* It is nevertheless possible, in a polydisperse system, that longer chains terminally reptate along a fatter tube than shorter chains, because $\Psi_{min}(t)$ may have decreased (and a_T increased) by the time the longer chains reptate.

A further point is necessary here: during "supertube" relaxation [i.e., when $\phi_{ST}(t) > \phi(t)$], we keep $\Psi_{min}(t)$ constant at its initial value from the start of the supertube relaxation. Our picture of CR Rouse relaxation is that of a thinner tube exploring the current fat tube via CR while keeping the thinner tube diameter constant: stress decay from CR is handled here by the time evolution of ϕ_{ST}. Allowing $\Psi_{min}(t)$ to change during this time would allow the CR additionally to contribute to speeding up of reptation, thus double counting some of the stress decay (which should not be allowed). Accounting for this is significant predominantly for chains with a small number of entanglements (i.e., preventing them from relaxing too fast within the algorithm).

In general, once an optimal reptation tube diameter a_T is found, $\Psi_{min}(t)$ will then typically remain at a constant value until $a_{eq}(t)$ reaches another, more optimal tube diameter. Considering a reptation dominated relaxation of bimodal blends (i.e., when the relaxation from CLF can be neglected), with a single CR time $\tau_{CR} \equiv \tau_{d,s}$, if $\tau_{d,s} \gg \tau_e/\phi_S^2$ and $B_\zeta = 1$, the analysis here agrees with the theory of Viovy and co-workers [14,28] deciding simply between reptation in thin or fat tubes, provided we neglect the small difference between ϕ_{ST} and ϕ_{eq}. Here, $\tau_{d,s}$ is the reptation time of the short chains, and ϕ_S is the weight fraction of the short chains.

F. Contour length fluctuation

To deal with CLF in a constantly evolving tube diameter, we follow the analysis by Read *et al.* [14]. A crucial feature of this is the distinction between (i) the optimal tube for chain transport *along* the tube (CLF requires chain sections to fluctuate back and forth along the tube over multiple tube diameters) and (ii) the tube in which chains can locally equilibrate, giving freedom to access deeper CLF through

equilibrium fluctuation. Hence, in the analysis for binary blends by Read *et al.* [14], for some blends local equilibration is possible in the fat tube (so that CLF occurs to a depth allowed by the fat tube) while the rate of CLF remains controlled by chain transport along the thin tube. We now generalize this to the case of nested tubes with multiple CR times.

The amount of chain end relaxed by CLF at a certain time t can be viewed as the number of monomers capable of moving coherently at that time. We assume that at t, the optimal tube for translational motion of chain subsections along the tube is given by the optimal tube diameter for reptation, $a_T \equiv a_0\phi_T^{-\alpha/2}$. The tube diameter in which monomers can locally equilibrate via CR is the current equilibrium tube diameter $a_{eq}(t) \equiv a_0\phi_{eq}^{-\alpha/2}(t)$. The translational friction coefficient for motion along the contour of tube diameter a_T can be mapped onto an effective friction constant for motion along the smoother contour of the current equilibrium tube diameter $a_{eq} \geq a_T$ as

$$\zeta_{CLF} = \zeta_T \frac{\phi_T^\alpha}{\phi_{eq}^\alpha}. \tag{22}$$

Hence, making use of Eq. (20) evaluated at its minimum,

$$\frac{\zeta_{CLF}}{\zeta_0} = \frac{\zeta_T}{\zeta_0}\frac{\phi_T^\alpha}{\phi_{eq}^\alpha} = \frac{\Psi_{min}(t)}{\phi_{eq}^\alpha(t)}. \tag{23}$$

The number of monomers that can participate in coherent fluctuation is estimated by inverting the Rouse time of these monomers as

$$n(t) = \sqrt{\frac{3\pi^2 k_B T}{\zeta_{CLF}b^2}}\sqrt{t} = N_e\sqrt{\frac{\zeta_0}{\zeta_{CLF}}}\sqrt{\frac{t}{\tau_e}}. \tag{24}$$

Following Read *et al.* [14], these $n(t)$ monomers have a collective friction constant $n(t)\zeta_{CLF}$, and thus a diffusion constant $(k_B T)/(n(t)\zeta_{CLF})$. Consequently, the rate of increase in the mean-squared displacement $\left\langle l_{a_{eq}}^2 \right\rangle$ of the end monomer via this correlated diffusion measured along the current tube diameter a_{eq} is, at the current time t,

$$\frac{d}{dt}\left\langle l_{a_{eq}}^2 \right\rangle = \mathcal{C}_1\frac{k_B T}{n(t)\zeta_{CLF}} = \mathcal{C}_1\frac{a_0^2}{3\pi^2}\sqrt{\frac{\zeta_0}{\zeta_{CLF}}}\frac{1}{\sqrt{t\tau_e}}$$
$$= \mathcal{C}_1\frac{a_0^2}{3\pi^2}\frac{1}{\sqrt{t\tau_e}}\sqrt{\frac{\phi_{eq}^\alpha(t)}{\Psi_{min}(t)}}. \tag{25}$$

Here, $\mathcal{C}_1$ is a numerical constant. Mapping displacement $l_{a_{eq}}$ along the tube at a_{eq} onto displacement z along a_0 (measured in the number of entanglements) $\left\langle l_{a_{eq}}^2 \right\rangle = \phi_{eq}^\alpha(t)a_0^2\langle z^2\rangle$.

So,

$$\frac{d}{dt}\langle z^2 \rangle = \frac{\mathcal{C}_a}{\sqrt{t \tau_e}} \frac{1}{\sqrt{\phi_{eq}^{\alpha}(t)\Psi_{\min}(t)}}. \tag{26}$$

Here, we have absorbed a factor of $1/3\pi^2$ in the new numerical prefactor $\mathcal{C}_a$. Since ϕ_{eq} is a monotonically decreasing function of time, CLF is most efficient in the current (widest available) tube. CLF is also accelerated when CR enhances the translational motion along fatter tubes, as captured by $\Psi_{\min}(t)$. We retrieve the familiar Doi and Edwards [3] expression for CLF if we integrate the equation assuming $\phi_{ST} = 1$ at all times (only thin tube is relevant for relaxation) and $\mathcal{C}_a = (2/3\pi^{3/2})$. Anticipating the advantage of logarithmic time steps,

$$\frac{dz}{d\ln\left(\frac{t}{\tau_e}\right)} = \frac{\mathcal{C}_a}{2z} \frac{1}{\sqrt{\phi_{eq}^{\alpha}(t)\Psi_{\min}(t)}} \sqrt{\frac{t}{\tau_e}}. \tag{27}$$

G. Transition from CLF to reptation relaxation

In previous works, especially the Hierarchical model and BoB models for predicting branched polymer viscoelasticity [24,25], the transition from CLF to reptation is handled by allowing CLF to continue, increasing $z(t)$ for each polymer, up until the reptation time accelerated by CLF as in Eqs. (19) and (21). Although appealing, this recipe unfortunately leads, in practice, to far deeper CLF and consequently faster reptation than is correct (for example, in comparison of the BoB and Hierarchical models to predictions for monodisperse polymers from Doi and Edwards [3] or analysis by Likhtman and McLeish [9]). This issue was highlighted by Shchetnikava *et al.* [39] who noted the overprediction of CLF in both Hierarchical model and BoB models.

A more correct scaling argument (see, e.g., [5]) is to compare the time to relax to depth z by CLF with the time to reptate the center of mass by distance z (measured in thin tube entanglement units). When the chain segment currently relaxing via CLF could have relaxed via reptation faster, the dominant relaxation mechanism changes from contour length fluctuation to reptation. If the segment z is reached via CLF at time t_c, we switch to reptation if

$$\mathcal{K}_R 3\mathcal{Z}(2z)^2 \Psi_{\min}(t_c) \le t_c. \tag{28}$$

Here, $\mathcal{K}_R$ is an order one constant. For a given chain, once the inequality of Eq. (28) is satisfied, the chain is assigned a reptation time according to Eq. (21) evaluated at $t = t_c$ (including the possible acceleration due to the availability of wider tubes accessible at this time). From this time onward, CLF relaxation is terminated for this chain and relaxation happens by the reptation spectrum (including higher mode contributions). Further relaxation of other chains does not change the assigned reptation time (though we leave the possibility open for terminal relaxation via total loss of entanglement described below).

For clarity, we emphasize the difference between this "new" prescription and that used previously. In the BoB and Hierarchical models, the depth of CLF increases continually right up to the reptation time at τ_d; the final reptation time was determined using this maximal degree of CLF to shorten the distance required to repate. In contrast, in the present model, CLF only proceeds up to the point where it becomes faster to relax to depth z by center of mass reptation motion. This crossover occurs much earlier than the reptation time (at the chain Rouse time for monodisperse chains, which is the natural time scale for CLF motion). Consequently, CLF effects are much smaller in the present model as compared to the BoB and Hierarchical models.

For pure reptation (without CLF in fixed tube diameter), the fraction of tube segment occupied as time t is given by

$$\mu_{rept}(t) = \frac{8}{\pi^2} \sum_{p,odd} \frac{1}{p^2} e^{-p^2 \frac{t}{\tau_{d,a_0}}}. \tag{29}$$

If, for a particular chain, the reptation time is assigned at t_c with the unrelaxed length of the chain as $\mathcal{Z}_R \equiv \mathcal{Z} - 2z(t_c)$, the maximum number of modes is selected from $p_{max} = \text{int}(\tau_d/t_c)$. The prefactor $8/\pi^2$ is changed to the inverse of the finite sum

$$\mathcal{S}_R \equiv \sum_{p,odd=1}^{p_{\max}} \frac{1}{p^2}. \tag{30}$$

Each exponential term in the sum is obtained via a step relaxation in $\phi(t)$ occurring at $\tau_{d,p} \equiv (\tau_d/p^2)$. In practice, at time $\tau_{d,p}$, we increase $z(t)$ by $(1/2)\mathcal{Z}_R/(p^2 \mathcal{S}_R)$ giving the desired effect in Eq. (3).

H. Loss of entanglement

When the current tube diameter becomes comparable to the size of a polymer ($\mathcal{Z}\phi_{ST} \simeq 1$), the polymer is no longer constrained by the tube constraints and the remaining modulus from this chain is considered to relax with the current time scale.

I. Subtube diameter relaxation

A part of modulus can relax by comparatively rapid rearrangement of the Rouse beads from tension equilibrium along the tube axis. We use the form of Likhtman and McLeish to describe this longitudinal Rouse contribution to the relaxation moduli as

$$G_L(t) = G_N^0 \sum_{i,\mathcal{Z}_i > \mathcal{Z}_u} \frac{w_i}{4\mathcal{Z}_i} \sum_{p=1}^{\mathcal{Z}_i-1} e^{-\frac{p^2 t}{\mathcal{Z}_i^2 \tau_e}}. \tag{31}$$

Here, w_i is the weight fraction of polymer i with $\mathcal{Z}_i$ entanglements and the sum over i only includes the entangled chains (see Sec. II J). Relaxation faster than τ_e within the Rouse bead picture is handled by considering the internal Rouse

contribution as

$$G_{IR}(t) = G_N^0 \sum_{i, \mathcal{Z}_i > \mathcal{Z}_u} \frac{5 w_i}{4 \mathcal{Z}_i} \sum_{p=\mathcal{Z}_i}^{N_e \mathcal{Z}_i} e^{-\frac{2p^2 t}{\mathcal{Z}_i^2 \tau_e}}. \qquad (32)$$

We incorporate fast glassy relaxation contribution as a single stretched exponential decay, [40,41]

$$G_g(t) = \left(G_\infty - \frac{5}{4} G_N^0 \right) e^{\left(\frac{t}{\tau_g} \right)^{\beta_g}}. \qquad (33)$$

Here, G_∞ is the glassy modulus, τ_g is the "α-relaxation" time, and the exponent $\beta_g < 1$ controls the stretched exponential decay observed experimentally. We assume that all these relaxation processes do not affect the long time relaxation described by the tube model and the contribution from these fast processes is added separately to the stress relaxation from the tube model in Eq. (2).

J. Relaxation of short unentangled chains

While our description is developed for well-entangled chains, experimental blends and polydisperse melts often contain a significant fraction of short unentangled chains. We hypothesize that the stress decay from chains with $\mathcal{Z} < \mathcal{Z}_u$ is described by a simple Rouse form and additive to the polymeric stress

$$G_R(t) = \frac{5 G_N^0}{4 \mathcal{Z}} \sum_{i, \mathcal{Z}_i \leq \mathcal{Z}_u} \sum_{p=1}^{N_e \mathcal{Z}} e^{-\frac{2p^2 t}{\mathcal{Z}^2 \tau_e}}. \qquad (34)$$

The effect of these short chains on the long molecules is modeled by considering the entire weight fraction carried by chains with $\mathcal{Z} < \mathcal{Z}_u$ relaxing with time scale τ_e in the calculation of the decay of ϕ_{ST}. Here, $\mathcal{Z}_u$ is an order one parameter.

III. RESULTS AND DISCUSSION

A. Uncertainty of experimental results and fitting the model parameters

The model developed here involves a number of parameters that, in principle, can be determined by fitting experimental observations. While a large number of studies on model (narrow molar mass distribution) polymers and their blends are available in the literature, an objective optimization of the parameters by fitting the experimental observations is problematic due to experimental uncertainties about the polymer characterizations, and the presentation of the relaxation data. This is exemplified by examining the molar mass dependence of the zero shear viscosity for a series of nominally 1,4 polyisoprene (PI) shown in Fig. 3. These polymers were anionically synthesized and were characterized as having a low polydispersity. Auhl et al. [42] and Abdel-Goad et al. [43] reported their zero shear viscosity data at 25 °C. The data from Watanabe and co-workers [18,44–46] were obtained by fitting the low-frequency dynamic viscosity to the Cross model and shifting
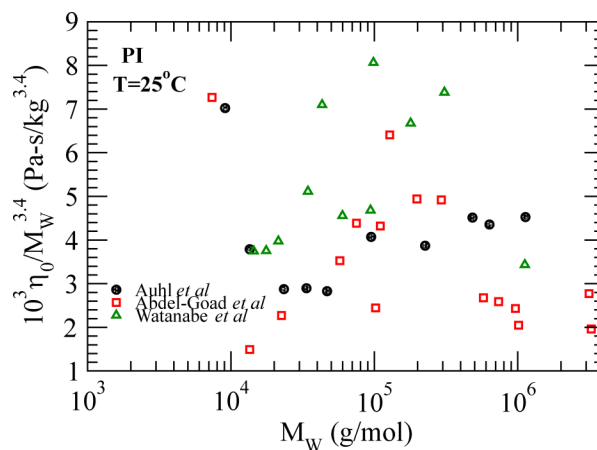

FIG. 3. Scaled zero-shear viscosity for various 1,4 polyisoprenes.

the values to 25 °C with the reported time-temperature superposition (TTS) parameters. The viscosity in this plot is scaled by $M_W^{3.4}$ to mitigate the dominant molar mass dependence so that the differences between the samples are prominent. Here, our expectation is not that all samples should lie on a horizontal line, because in practice the viscosity deviates slightly from the $M_W^{3.4}$ power law, especially at the low molecular weight end. Rather, Fig. 3 allows us to compare viscosity values obtained for polymers of nominally the same molecular weight. For example, concentrating at $M_W \simeq 10^5$ g/mol, Fig. 3 shows that the viscosities of the four different samples differ by up to a factor of 4. A conventional view of the plot of viscosity versus molecular weight, along with theoretical predictions, is shown in Fig. 6. Here, the logarithmic scale hides the differences between measurements that are more evident in Fig. 3.

The significant scatter in the zero-shear viscosity in Fig. 3 can be due to multiple uncertainties about the samples and the measurements. First, routine molar mass determination from gel-permeation chromatography can have large uncertainty and can vary systematically between the different groups because of different protocols [47]. For polydisperse samples, the detailed shape of the molar mass distribution may be important but is seldom reported in the literature. Second, the "headline" chemistry hides the fact that different samples can have different microstructures (and possibly different amounts of solvents) resulting in different responses [48–50]. Finally, the experimental results are normally presented as composite master curves by combining results from experiments at different temperatures [51]. Different protocols used by different groups can result in significantly different master curves from the same raw data. Since η_0 values were estimated from the dynamic viscosity curves, any difference in constructing the master curves also will affect the value of η_0. Note that an uncertainty in the molar mass of around 30% alone can explain the scatter in η_0 at $M_W \simeq 10^5$ g/mol. The uncertainty in the experimental data is expected mostly due to "systematic errors"—for example, a certain separation column in the GPC measurement or a certain protocol for constructing the master curves. The somewhat smaller scatter in the data from Auhl et al. [42] is probably because all the molar masses of the samples were determined in successive

measurements on the same GPC column and the rheology measurements were performed on the same machine within a short time. Thus, although we still expect errors in these measurements, the systematic errors for these samples are likely to be correlated and give deviations in an identical direction.

In view of the uncertainties associated with the available experimental data, we have first reduced the number of model parameters by assigning reasonable *a priori* values to a subset of parameters, used results from available computer simulations to determine a few of the parameters, and used selected experimental data to determine the remaining parameters. Of course, the parameters so determined cannot describe *all* the experimental data that we consider in this paper in view of the differences between the experiments exemplified in the scatter of the zero-shear viscosity. In describing some of the experimental data, we needed to reassign different molar masses (and polydispersity) than the reported values. Also, in some cases, the data are best described by assigning somewhat different values of the entanglement times for different samples of the same headline chemistry. These changes in the molar mass and variations in τ_e are clearly stated where they have been used.

An alternative possibility to account for the uncertainties in the experimental results in our modeling would be to adjust parameters within likely ranges (instead of using single well-defined values) and to present theoretical predictions with confidence bands on each plot. We give an example of such a plot in Appendix C. However, we believe that the majority of the experimental uncertainty is from systematic and correlated reasons (e.g., an error in parameterization of the pure sample is carried over in a correlated way into blends from that sample). So, constructing a cost function to minimize for fitting the model parameters is problematic. Further, presenting simple confidence bands in predictions across several graphs is misleading when we expect those errors to be correlated. Finally, the resulting predictions would have uncertainties larger than the subtle changes in the viscoelastic and dielectric responses that we are interested in describing. The confidence bands in many of the blends considered in this paper would be much wider than the separation between individual concentration results, as is illustrated in Appendix C. Hence, for the majority of the paper, we show sharp predictions using only a single value for the material-dependent parameters and ignoring the uncertainties; nevertheless, the reader should be aware of these uncertainties and that they manifest themselves in a correlated way across the data.

We assume that certain parameters are chemistry independent and first detail our considerations in assigning their values in Subsection III B. The chemistry dependent material parameters are introduced separately along with results for monodisperse polymers in Subsection III C.

B. Chemistry independent parameters

We use the tube dilation exponent $\alpha = 1$, consider molecules to be unentangled if $\mathcal{Z}_U \leq 1.5$, and consider

molecules to relax completely by CR when $\mathcal{Z}\phi_{ST} = 1$. We set the constant B_ζ connecting CR time to friction as 2.0 and use the same value for the constant A_{eq} that determines delay in accessing wider tubes for translational diffusion. The choice of $\mathcal{Z}_U$, along with modification of short-time CLF [Eq. (37)], determines the crossover of the slope of molar mass dependence of the zero shear viscosity from unentangled to entangled behavior. A different choice of $\mathcal{Z}_U$ would require a different modification to the short-time CLF than reported here. The results remain qualitatively unchanged with ∼10% variations in B_ζ, or A_{eq}, and we fix these parameters as 2 based on the Rouse result of a factor 2 difference between the stress and orientation relaxation times.

We force predictions from our model for $\mu(t)$ to match the stochastic simulation results of Likhtman and McLeish [9] (LM model) in the long-chain limit. This fixes the prefactor $\mathcal{C}_a$ for CLF, and the parameter $\mathcal{K}_R$ associated with transition from CLF to reptation. Likhtman and McLeish [9] found that their simulation results for $\mu(t)$ can be described as $\mu(t) = 1 - (c_\mu/\mathcal{Z})(t/\tau_e)^{1/4}$ for $t < \tau_R$ with $c_\mu = 1.5$ and the reptation time can be expressed as $\tau_d = 3\mathcal{Z}^3 f(\mathcal{Z})\tau_e$. The function f was fitted by them as

$$f(\mathcal{Z}) = 1 - 2C_1/\sqrt{\mathcal{Z}} + C_2/\mathcal{Z} + C_3/\mathcal{Z}^{3/2}, \qquad (35)$$

with $C_1 = 1.69$, $C_2 = 4.17$, and $C_3 = -1.55$. Results for $\mu(t)$ from our model for long chains in a fixed tube for $t < \tau_R$ match that of Likhtman and McLeish [9] with $\mathcal{C}_a = 0.189$. With a constant parameter $\mathcal{K}_R$ determining the switch between the CLF to reptation dominated relaxation [Eq. (28)], the reptation time in the absence of CR is

$$\tau_d = 3\mathcal{Z}^3 \left[1 - \frac{4\mathcal{C}_a\sqrt{3\mathcal{K}_R}}{\sqrt{\mathcal{Z}}}\right]^2 \tau_e. \qquad (36)$$

The leading order dependence of τ_d on $\mathcal{Z}$ can be matched with the LM model using $\mathcal{K}_R = 1.664$. However, the differences in the higher order terms result in significant underestimates in the value of τ_d for moderately entangled chains as compared to the predictions of the LM model (and experiments). In order to describe the relaxation of moderately entangled polymers in the same framework, we modify the short-time CLF by introducing a time-dependence in $\mathcal{C}_a$ as an approximation of step function about τ_e in the logarithm of time as

$$\mathcal{C}_a(t) = \mathcal{C}_{a,0} + \frac{\mathcal{C}_{a,\infty} - \mathcal{C}_{a,0}}{1 + (\tau_e/t)^{\epsilon_a}}. \qquad (37)$$

The long-time coefficient for CLF $\mathcal{C}_{a,\infty}$ is chosen to be 0.189 such that for sufficiently long chains the predictions from our algorithm for $\mu(t)$ in the absence of CR are indistinguishable from the LM model predictions. We use experimental results from Auhl *et al.* [42] on a series of PI to fit the short-time coefficient $\mathcal{C}_{a,0} = 0.02$ and the exponent $\epsilon_a = 0.42$ controlling the sharpness of transition to the long-time behavior.

Note that these values overcompensate the deviation from the LM predictions for the $\mu(t)$ for moderately entangled chains and follows the experimental results closely down to unentangled PI polymers. With our chosen parameters, the higher order coefficients in the expansion of $f(\mathcal{Z})$ in Eq. (35) are different from those of Likhtman and McLeish and are $C_2 = 4.5$ and $C_3 = -1.98$.

We use the rheology results of [13] on PI binary blends and dielectric and mechanical relaxation of [44,45] data on PI binary blends to assign $\delta_{CR}^{\infty} = 0.3$ as the fractional drop in ϕ_{ST} for long CR times. It is notable that recasting this value in terms of A_ζ, the proportionality constant between CR friction and time scale of CR [Eq. (7)], this value for δ_{CR}^{∞} gives $A_\zeta = 1.25$, which is substantially larger than the value 0.047 obtained by Read *et al.* [14] from slip-spring simulations and apparently confirmed by experimental observations of Malo de Molina *et al.* [52]. The simplified model of Read *et al.* [14], when applied to experimental data, assumes that the CR time of the short chains is identical to their terminal reptation time. In contrast, the detailed modeling proposed here considers the full spectrum of CR times including CR from CLF (which is a significant fraction of CR for moderately entangled chains and significantly faster than reptation). Both the simplified model of Read *et al.* [14] and our detailed model in this work are applied to describe the same experimental results (i.e., they must assign the same total friction from CR). Hence, to match the same experimental data, a small value of A_ζ is needed for the simplified model but a larger one is needed in the present work. In Appendix D, we show that our model with $A_\zeta = 1.25$ describes the binary blend of [52] and explicitly show how CLF makes a large correction to the assumption in the model of Read *et al.* [14] of a single CR relaxation time. In this context, it is notable that the present model still predicts a small value for the critical Graessley parameter for crossover between relaxation by CR or reptation for dilute long chains in a binary blend (see Fig. 9). Nevertheless, the value of the constant A_ζ and its relation to constraint release rates from realistic polymers deserves further investigation in future work.

We summarize the chemistry independent parameters in Table I along with reference to the equations where they appear in the text. We note that $\mathcal{Z}_U$ and the short time correction to CLF determine the "crossover molar mass," M_X, between the entangled and entangled behavior. The ratio of

M_X and M_e is found in experiments to mildly depend on the chemistry. Hence, $\mathcal{Z}_U$ and the short-time correction to CLF should also have some dependence on the chemistry. In our modeling, we have fitted these parameters based on PI and used the same values for PB and PS.

C. Material-dependent parameters and results for monodisperse polymers

We begin with a consideration of fitting to data from near-monodisperse polymers, since these form a base case allowing us to fix parameters for a later description of polydisperse materials. Note that we fully account for polydispersity even for these narrowly distributed materials.

We use a series of well-characterized narrowly distributed PI from Auhl *et al.* [42] to determine the M_e, τ_e, and G_N^0 for polyisoprene. These samples also serve to determine the early-time modification of the prefactor to CLF. Figure 4(a) shows the viscoelastic moduli (symbols) from [42] and our predictions (lines) with $M_e = 4.35\,\text{kg/mol}$, $\tau_e = 1.3 \times 10^{-5}$ s, and $G_N^0 = 476\,\text{kPa}$. Note that for the 23k, 34k, 226k, and 483k samples we follow the molecular weight labels from [13]. The molecular characteristics of these samples from [42] are 12k [$M_W = 13.5\,\text{kg/mol}$, polydispersity index (PDI) = 1.04], 23k (23.4, 1.03), 34k (33.6, 1.03), 90k (94.9, 1.03), 226k (225.9, 1.03), 483k (483.1, 1.03),

TABLE I. Model parameters independent of polymer chemistry.

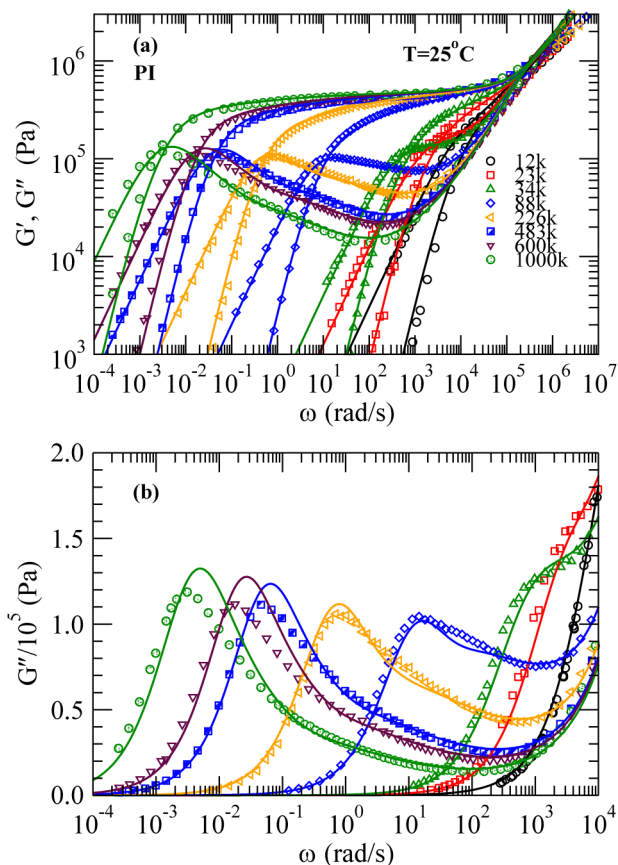| Parameter	Value	
α	1	Eq. (1)
δ_{CR}^{∞}	0.3	Eqs. (9) and (10)
B_ζ	2	Eq. (14)
A_{eq}	2	Eq. (17)
B_{eq}	10	Eq. (17)
$\mathcal{C}_{a,\infty}$	0.189	Eqs. (27) and (37)
$\mathcal{C}_{a,0}$	0.02	Eq. (37)
ϵ_a	0.02	Eq. (37)
$\mathcal{K}_R$	1.664	Eq. (28)
$\mathcal{Z}_U$	1.5	Sec. II J

FIG. 4. (a) Storage and loss moduli of PI samples shifted to an isofrictional state at 25 °C from [42] along with predictions from our model. (b) Zoomed view of the loss moduli of the same samples presented in log-linear scale to highlight the terminal relaxation.
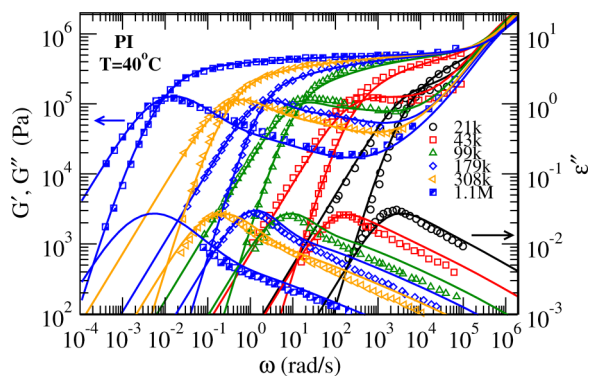
FIG. 5. Mechanical and dielectric relaxation moduli of PI samples from [46] along with predictions from our model.

FIG. 6. Zero-shear viscosity as a function of the molar mass for 1,4 polyisoprenes.

600k (634.5, 1.03), and 1000k (1131.0, 1.05). The zoomed view of the loss moduli in Fig. 4(b) shows that for long chains we overpredict the height of the reptation peak by about 10%.

The choice of τ_e depends on the high-frequency glassy relaxation to some extent [40,41]. However, for many polymers, the high-frequency relaxation of local conformation (segmental modes) and the low-frequency relaxation of chain conformation (chain modes) follow different temperature dependencies for the horizontal shift factor [53]. While a reasonably smooth master curve can be obtained by combining different temperature measurements [54], the resulting master curve will depend on the details of the fitting procedure. For, our description of PI, we fix $G_\infty = 10^9$ Pa, and $\tau_g = 7 \times 10^{-11}$ s from the stress and dielectric relaxation experiments, respectively, from the work of Mohamed et al. [55]. We fix the stretching exponent $\beta_g = 0.37$ to best describe the slope of the high-frequency elastic moduli in Fig. 4. With the uncertainty about the validity of TTS and lack of extensive good quality glassy responses in the literature, we assume that the high-frequency contribution simply shifts in proportion to τ_e if the reference temperature of 25 °C is changed.

Similarly, Fig. 5 shows both the mechanical viscoelastic response and the dielectric loss modulus for a series of PI samples from Matsumiya et al. [46]. The predictions for ϵ'' are calculated as $\mu''/10$. Here, we used slightly different

values of τ_e for each of the different samples to describe the data (see Table II). A modification such as this is required to account for the differences in zero shear viscosity between different samples evident in Fig. 6, both in terms of apparent discrepancy of the overall trend between the Matsumiya and Auhl data, but also to account for variation from one sample to the next. A different value of τ_e might represent a slightly different microstructure. An alternative, here, would be to attribute the scatter in data to differences in calibration and variation in GPC measurements between groups, or to different TTS procedures. Nevertheless, we have found that the simple expedient of allowing a small change in τ_e and of making correlated changes for blends of these materials (see below) allows a consistent description of both the monodisperse samples and their blends. In the present work, this was particularly important to us since these PI samples and their blends were used to determine δ_{CR}^∞. So, we matched G' from the highest available frequency to the crossover frequency as closely as possible for these samples with a variable τ_e. This procedure ensures that differences in microstructure or T_g do not affect the fitting of δ_{CR}^∞. Nevertheless, the range of variation in τ_e is rather small and in most cases using a single τ_e will result in visually very similar plots (the symbol sizes in the figures in this paper are of similar dimensions as the

TABLE II. Molar masses of PI from Watanabe et al.

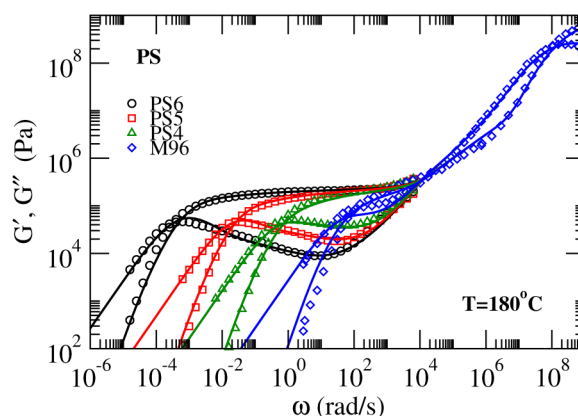| Label	M_W (kg/mol)	PDI	τ_e at 40 °C (10^{-6} s)
L14k	14.4	1.03	5.2
L18k	17.6	1.04	6.5
L21k	21.4	1.04	6.5
L34k	34.4	1.04	6.8
L43k	43.2	1.03	9.9
L60k	59.9	1.05	6.8
L94k	94.0	1.04	5.9
L99k	98.5	1.04	8.7
L179k	179.0	1.02	6.8
L308k	308.0	1.08	7.6
L626k	626.0	1.06	7.0
L1M	1120.0	1.13	5.9

FIG. 7. Storage and loss modulus of PS from Schausberger et al. [56] and Matsumiya et al. [57] along with predictions. The data from M96 have been shifted to 180 °C.
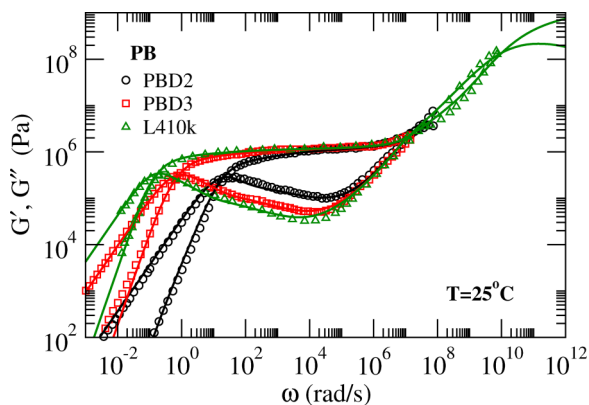
FIG. 8. Storage and loss modulus of PB PBD2 and PBD3 from Li *et al.* [59] and 410k from Wang *et al.* [16] along with predictions at 25 °C.

variation in τ_e used): i.e., once δ_{CR}^{∞} is determined, it is then possible to get reasonable looking predictions using a single τ_e value.

Of particular note in Fig. 5 is that we capture the offset (by roughly factor 2) between the peaks in dielectric and rheological loss modulus. This prediction is a direct result of using Eq. (4) for dielectric relaxation and Eq. (2) for stress relaxation, together with the step drop in ϕ_{ST} parameterized by δ_{CR} as outlined in Sec. II C. As a result, CR is predicted to increase the rate of stress relaxation. The use of Eq. (6) for stress relaxation would not produce this effect. We show the molar mass dependence of viscosity predicted from our model in Fig. 6 by considering a series of polymers with a narrow fixed polydispersity of 1.01. The parameters chosen for these predictions are the same as used in describing the PI samples in Fig. 4. We superpose literature data of various PI samples in the plot. Because of the logarithmic scale and since we have not removed the dominant $M_W^{3.4}$ scaling from the viscosity, the differences in the experimental data are not so evident as in Fig. 3, but are still visible on close inspection. The theoretical curve closely matches the Auhl data, as expected.

Turning to other polymer chemistries, Fig. 7 shows the dynamic modulus for PS6 (2.54M; 1.13), PS5 (757k; 1.09), and PS4 (292k; 1.09) at 180 °C from Schausberger *et al.* [56]. The molar masses of these samples were updated in a later publication [58]. The data for M96 (96.4k; 1.05) from

Matsumiya *et al.* [57] have been shifted from the reported 110 °C by scaling the frequency and modulus with factors 2.5×10^6 and 0.87, respectively. The parameters used for the predictions in Fig. 7 are $M_e = 12.87$ kg/mol, $\tau_e = 2.2 \times 10^{-4}$ s, $G_N^0 = 220$ kPa, $\tau_g = 1.3 \times 10^{-9}$ s, $G_\infty = 1.2$ GPa, and $\beta_g = 0.39$.

Figure 8 shows the dynamic modulus from two PB samples from Li *et al.* [59]. The synthesis of these samples resulted in significant end-linking. GPC results of PBD2 are described as a blend of 10% 147k (PDI=1.13) and 90% 94k (1.02). The PBD3 sample is described as a blend of 10% 292.5k (1.03), 40% 268k (1.03), and 50% 253k (1.03). The figure also shows the results of 410k (411.5k; 1.01) from Wang *et al.* [16] that extend significantly in the glassy regime. This dataset was shifted by scaling the frequency and modulus with factors 0.859 and 1.01, respectively. The predictions in Fig. 8 used $M_e = 1.63$ kg/mol, $\tau_e = 2.5 \times 10^{-7}$ s, $G_N^0 = 1.2$ MPa, $\tau_g = 4.5 \times 10^{-12}$ s, $G_\infty = 1.2$ GPa, and $\beta_g = 0.32$.

We summarize the material parameters for all three chemistries in Table III. We quote values of τ_g and G_∞ as ratios of τ_e and G_N^0, respectively, in this table. In describing data from different reference temperatures, we have used Rouse scaling of the modulus shift (vertical shift in G_N^0 proportional to the product of density and absolute temperature) and change in τ_e (horizontal shift factor a_T). Our assumption that time-temperature superposition approximately holds requires τ_g and G_∞ to vary in the same way with temperature as τ_e and G_N^0, respectively, and their ratios need to be approximately temperature independent. In Table III, the τ_e values for PI, PB, and PS refer to those used in describing data presented in Figs. 4, 7, and 8, respectively. As discussed above, somewhat different values of τ_e are required to describe some of the other polymers considered in this paper. We include a range for the values of τ_e for each of these chemistries in Table III that we needed to describe all the different experimental data.

D. Binary blends of narrow molar mass distribution polymers

We turn now to binary blends composed of monodisperse polymers of two chain lengths. For each polymer chemistry, the structure of these melts can be characterized by three parameters: the molecular weight of the long and short polymers (which can be expressed in terms of the number of entanglements, Z_L and Z_S along long and short chains) and the volume fraction ϕ_L of long chains in the melt. This nevertheless produces a rich variety of modes for polymer motion, dependent on the degree to which long chains are restricted by entanglements with other long chains, and the relative rate of CR from short chains, as compared to other modes of long-chain motion. For a pure reptation description of polymer motion (i.e., ignoring CLF), Viovy *et al.* [28] proposed a two-dimensional projection of the three-parameter space: parameter $\tilde{Z}_L = Z_L \phi_L$ characterizes the degree to which long chains are entangled with themselves (assuming dilution exponent of one); the Graessley parameter $Gr = Z_L/Z_S^3$ characterizes the relative importance

TABLE III. Material parameters for 1,4 PI, 1,4 PB, and atactic PS at the shown reference temperature.

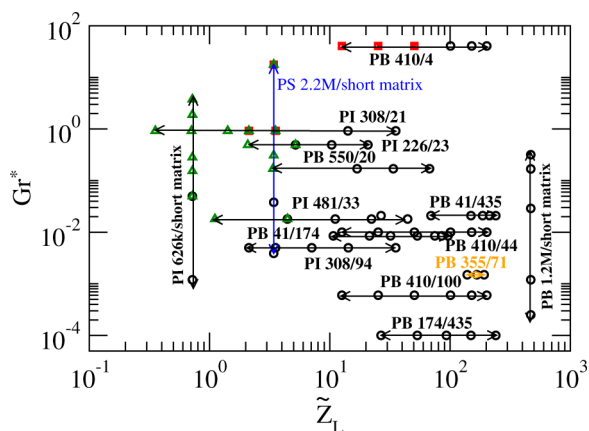|	1,4 PI	1,4 PB	a-PS
T_{ref} (°C)	25	25	180
M_K (g/mol)	113	105	720
M_e (g/mol)	4350	1630	12 870
τ_e (s)	1.3×10^{-5}	2.5×10^{-7}	2.2×10^{-4}
	[1.3–3]	[2.5–5.1]	[1.2–3.8]
G_N^0 (kPa)	476	1200	220
$\frac{G_\infty}{G_N^0}$	2100	1000	5455
$\frac{\tau_e}{\tau_g}$	1.86×10^5	5.56×10^4	1.69×10^5
β_g	0.37	0.32	0.39

FIG. 9. Location of the various bimodal blends modeled in this study on the Viovy diagram. The green triangles indicate cases where the terminal relaxation of the long component is via CR. The black circles and the red squares indicate cases where the long component relaxes by reptation in the thin or the fat tube, respectively. Because of small but finite polydispersity of the samples, in some cases, different molar mass components of the long chains access different terminal relaxation pathways.

of CR from short chains on the dynamics of the long chains. Small values of Gr correspond to slow CR (so that reptation along the thin tube dominates) while larger values of Gr correspond to faster CR, opening up other avenues for long-chain relaxation. This picture was modified by Read *et al.* [14] to include the additional effects of CLF, resulting in a
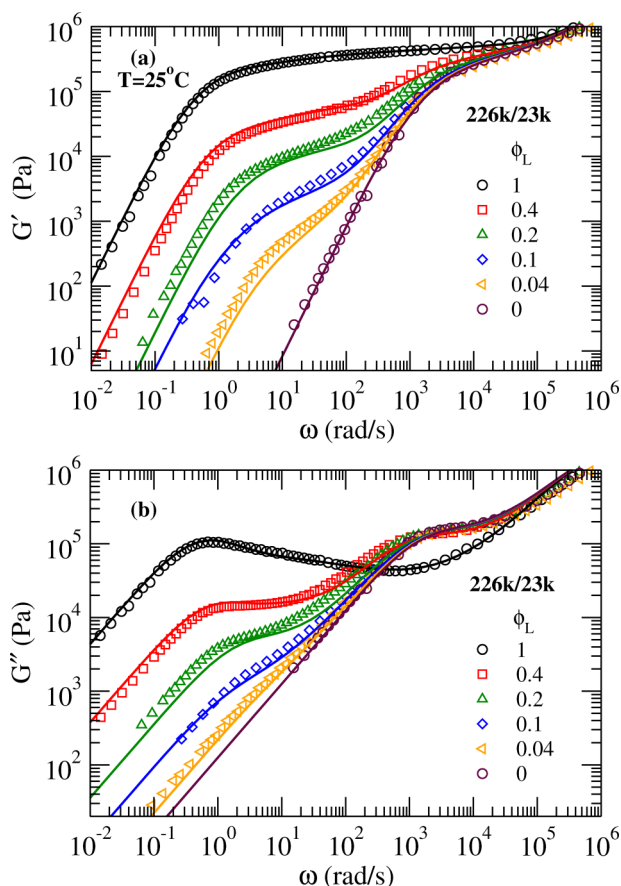
FIG. 10. Viscoelastic responses for PI 226k/23k blends from [13] at the shown weight fractions along with predictions.
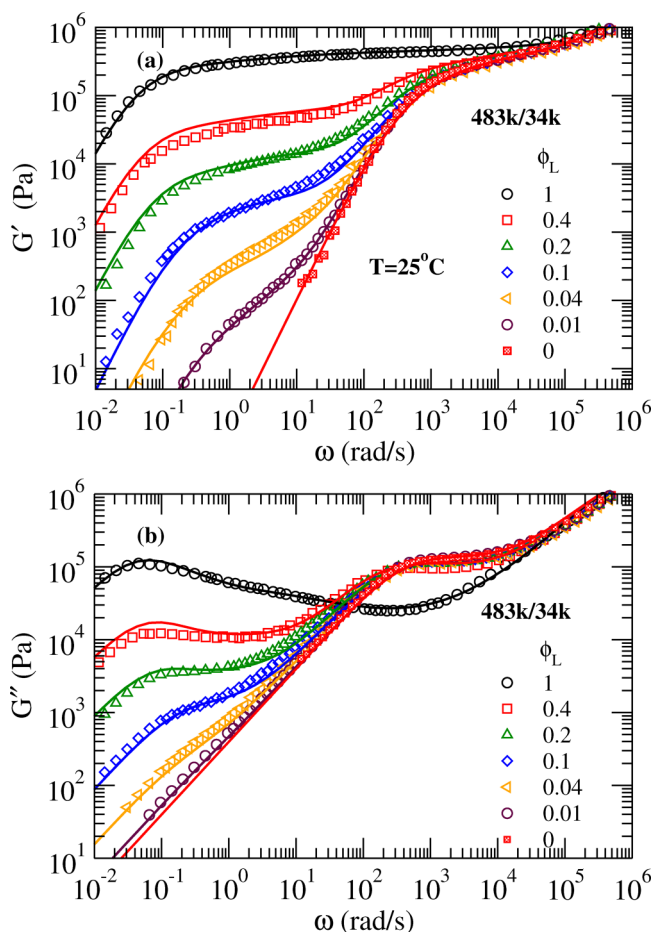
FIG. 11. Viscoelastic responses for PI 483k/34k blends from [13] at the shown weight fractions along with predictions.

suggested modification of the Graessley parameter to

$$Gr^* = \frac{Z_L}{3Z_S^3 f(Z_S)}, \quad (38)$$

where $f(\mathcal{Z})$ introduced in Eq. (35) is the Likhtman–McLeish [9] correction to reptation time due to CLF. We use results for monodisperse polymers from our model to estimate $f(\mathcal{Z})$ for the short chains in assigning Gr^* in this paper. Both Viovy *et al.* and Read *et al.* use the two-dimensional $(\tilde{Z}_L, Gr^*)$ space to map out regions where different dynamical behavior from long chains is expected, for example, where reptation is expected to be dominated by motion along thin or fat tubes. For summaries for this, see for example, [5,13,14,28].

For our purposes, we employ the suggested two-dimensional $(\tilde{Z}_L, Gr^*)$ map of parameter space as a means to ensure that we test our model against as wide a variety of different types of binary blend as possible. It is not sufficient to demonstrate predictions only in a small window of this space, where typically only one or two relaxation mechanisms are dominant. Accordingly, we show in Fig. 9 the two-dimensional $(\tilde{Z}_L, Gr^*)$ space populated by the locations of the various sets of data we investigate. It can be seen that these span a wide range of relative CR rates, as well as long
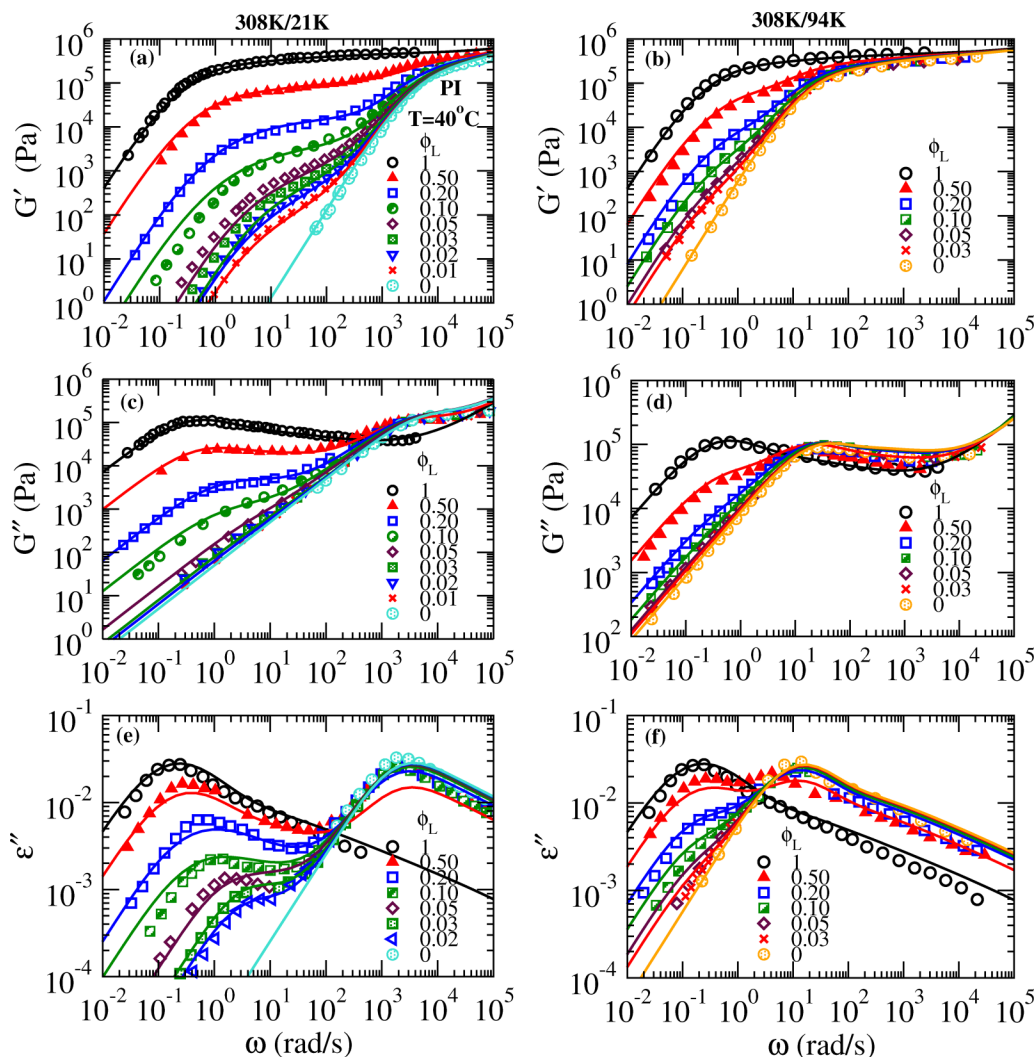
FIG. 12. Viscoelastic and dielectric responses for PI 308K/21K blends from Watanabe *et al.* [44] and for PI 308K/94K from Watanabe *et al.* [45] at the shown weight fractions along with predictions.

chains ranging from dilute to well entangled with one another.

We first consider several studies which employed two polymers of different molar masses and systematically varied the relative weight fraction of the components to vary $\tilde{Z}_L$ while keeping Gr^* fixed (horizontal lines in the Viovy diagram). Figures 10 and 11, respectively, show the viscoelastic responses of blends of PI 226k and 23k ($\mathrm{Gr}^* = 0.54$) and of PI 483k and 34k ($\mathrm{Gr}^* = 0.32$) considered by Read *et al.* [13]. We use identical values of τ_e, M_e, and G_N^0 for the predictions as we used for the monodisperse polymers considered in Fig. 4. In both cases, at the lowest concentrations of the long chains ($\phi_L = 0.04$), the long chains become unentangled in the supertube and the final relaxation of the long component is via disentanglement. At higher concentrations, the terminal relaxations of the long chains are via chain motion along the thin tube. With reduction in ϕ_L, the peak in G'' shifts to higher frequencies—the reduction in the reptation times in these cases is due to enhanced CLF in the fat tube [i.e., in terms of the notation of Eq. (27), $\Psi_{\min}(t)$ corresponds to chain motion along the thin tube, while $\phi_{eq}^\alpha(t)$ allows freedom for CLF taking place in the fat tube, as

described in [13] and [14]]. Our predictions capture shifts in both the frequency and modulus in the dynamic viscoelastic moduli without any additional fitting parameters.

Figure 12 shows the viscoelastic and dielectric responses for blends of PI 308K and either 21K (plots a,c,e) or 94K (plots b,d,f) from [44] and [45]. We show $\mu''/10$ as proxy for ϵ''. As with the predictions for the individual components, we have used slightly different values of τ_e for the different blends (τ_e between 6.2 and 7.2 μs for blends with 21k and between 5.9 and 6.5 μs for blends with 94K). The data for low concentrations of the long chains fit with the same values of τ_e as required to fit the pure short chains. The terminal relaxation of the long chains in the 308K/21K blend ($\mathrm{Gr}^* = 0.92$) is via CR for $\phi_L \leq 0.02$, via reptation in the fat tube for $0.03 \leq \phi_L \leq 0.1$ and via reptation in the thin tube for $\phi_L \geq 0.2$. With small values of the Graessley number ($\mathrm{Gr}^* = 0.005$, i.e., very slow CR), the long chains in the 308K/94K blend switch over to reptation in the thin tube from terminal relaxation by CR for $\phi_L \geq 0.03$.

Figure 13 shows the experimental data and predictions for a series of bimodal PB blends measured by Wang *et al.* [16]. The 410K long chains ($M_W = 411.5$ kg/mol, PDI=1.01) were
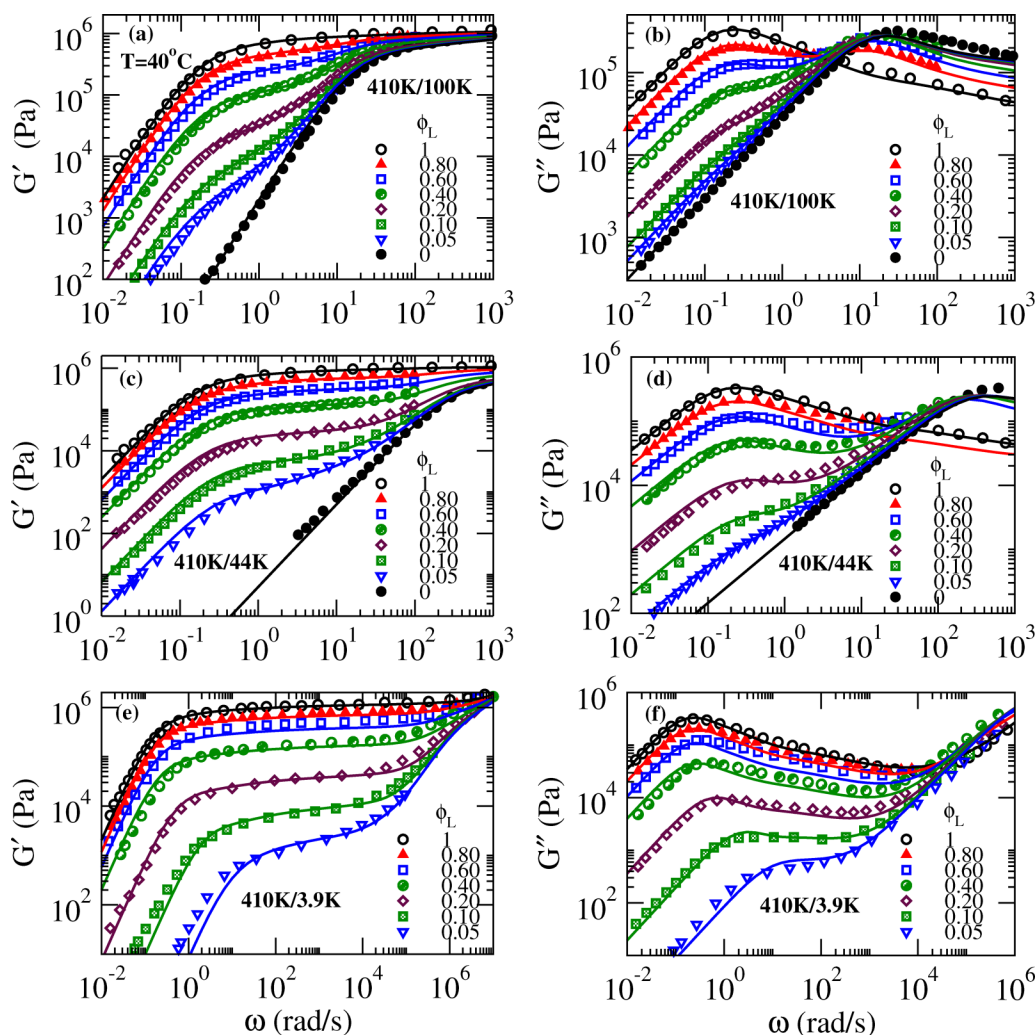
FIG. 13. Master curves for PB blends at the shown weight fractions from Wang *et al.* [16] along with predictions.

blended at 5, 10, 20, 40, 60, and 80% concentrations in different short chains resulting in $\tilde{Z}_L$ between 12.6 and 202. For these predictions, we use $\tau_e = 2.15 \times 10^{-7}$s at the reference temperature of the experimental data of $40\,^{\circ}$C. Using the TTS parameters from [59], this corresponds to $\tau_e = 4.4 \times 10^{-7}$s at $25\,^{\circ}$C, approximately 75% larger than those used for predictions in Fig. 8.

Figures 13(a) and 13(b), respectively, show the elastic and viscous responses with the 100K short chains ($M_W = 99.1$ kg/mol, PDI=1.01). With very small $\mathrm{Gr}^* = 6 \times 10^{-4}$, the terminal relaxation of the long chains are in the thin tube at all concentrations. The 410K chains also reptate in the thin tube at all concentrations in the blends with the 44K sample ($M_W = 43.9$ kg/mol, PDI=1.01) with $\mathrm{Gr}^* = 0.01$ shown in Figs. 13(c) and 13(d).

The blends with 3.9K ($M_W = 3.9$ kg/mol, PDI=1.1) in Fig. 13(f) have $\mathrm{Gr}^* = 40.8$ and show a transition from thin tube to fat tube reptation for the long chains as a function of the 410K concentrations. The long chains at concentrations 20% ($\tilde{Z}_L = 50.5$) or below reptate in the fat tube. The long chains at 40% ($\tilde{Z}_L = 101$) and higher concentration blends undergo reptation in the thin tube. This transition with increasing long-chain concentration, from reptation along fat tube to

reptation along the thin tube, is the expected behavior from the Viovy diagram [5,14,28]. The reason is that at higher long-chain concentrations the "fat tube" is not so fat and becomes longer and more tortuous than it was at low concentrations: thus, reptation along the fat tube becomes slower with increasing concentration. In contrast, reptation along the thin tube stays the same rate and eventually becomes the faster process.

The short species 3.9K in these blends have relatively high polydispersity (1.1). Assumption of a log-normal distribution suggests that 9.5 wt. % of the chains are below $1.5M_e$ and have been assumed to relax by unentangled Rouse dynamics in our calculations. For the 5% blend, the entangled chains below 9.1 kg/mol reptate in the thin tube. The resulting increase of the tube diameter makes the remaining high molar mass tail of the 3.9K species effectively unentangled. In the 10% blend, thin tube reptation is accessed by the entangled chains below 8.4 kg/mol in the 3.9K species. The remaining 0.4 wt. % of short chains having higher molar mass reptate in a fatter tube (of diameter much smaller than the fat tube accessed for reptation of the 410K species). This change from thin to fat tube reptation shifts to 7.7 kg/mol for the 20% blend (0.9 wt. % chains in the high molar mass tail of 3.9K species reptate in the fat tube). All entangled chains
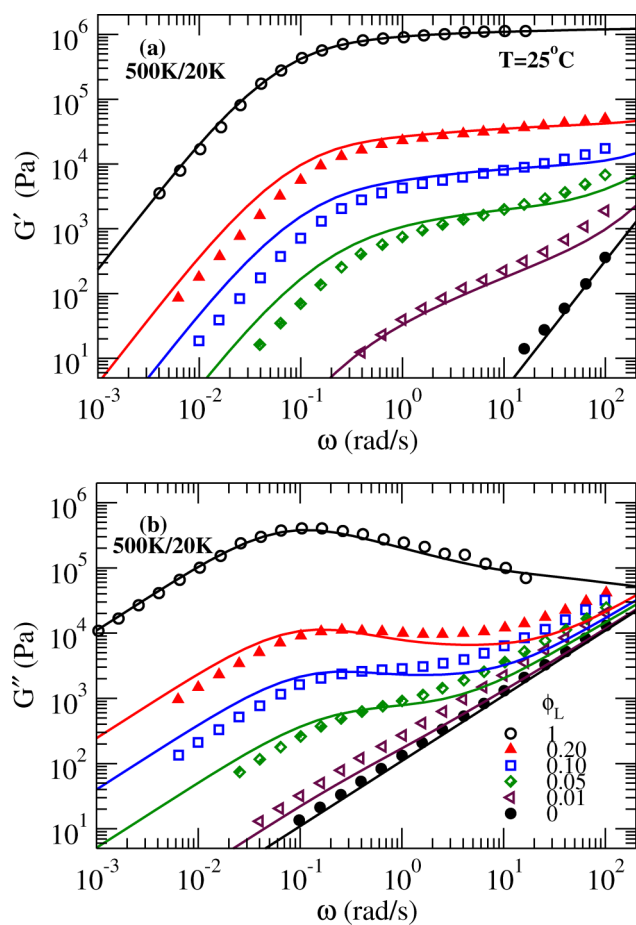
FIG. 14. Viscoelastic responses for PB 550K/20K blends from Park and Larson [17] at the shown weight fractions along with predictions.
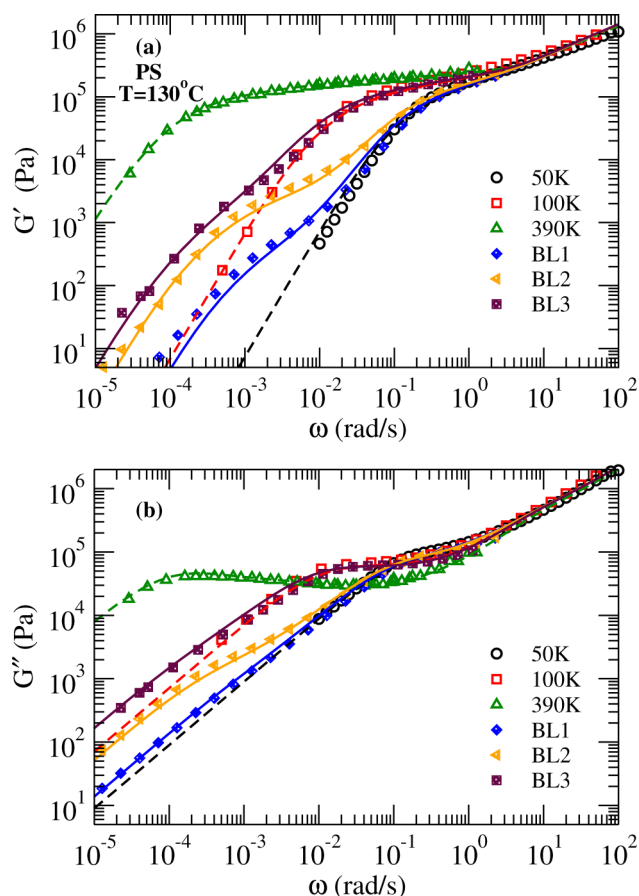

FIG. 15. Viscoelastic responses for PS 50K, 100K, and 390K and three blends from Nielsen *et al.* [60] along with predictions. The dashed and solid lines show predictions for the pure materials and the blends, respectively.

of the 3.9K species reptate in the thin tube for the higher concentration blends.

Figure 14 shows the experimental data on blends of PB 550K and 20K (Gr* = 0.17) from Park and Larson [17] along with our predictions. We have assumed a PDI=1.05 for the 550 kg/mol sample and a PDI=1.02 for the 20 kg/mol sample. The pure 550K sample experimental data were presented from measurements at 70 °C with the appropriate horizontal shift, but without any vertical shift. To compensate, our predictions for the pure 550K sample have been shifted vertically by a factor 1.116. These predictions use the same material parameters as used for the predictions in Fig. 8, specifically the same $\tau_e = 2.5 \times 10^{-7}$ s. At the lowest concentration of the long chains ($\phi_L = 0.01$), the long chains become unentangled in the fat tube before reptation can be accessed. The terminal relaxations of both the short and long species are reptation in the thin tube for all the higher concentration blends.

The dashed lines in Fig. 15 show the dynamic moduli for PS50K ($M_W = 51.7$ kg/mol, PDI = 1.026), PS100K ($M_W = 102.8$ kg/mol, PDI = 1.022), and PS390K ($M_W = 390$ kg/mol, PDI = 1.06) from Nielsen *et al.* [60]. Also shown with solid lines are dynamic moduli for three blends from the same reference: BL1 (4.02% PS390K in PS50K matrix, $\tilde{Z}_L = 1.22$, Gr* = 0.82), BL2 (14.37% PS390K in PS50K matrix, $\tilde{Z}_L = 4.35$, Gr* = 0.82), and BL3 (14.02% PS390K

in PS100K matrix, $\tilde{Z}_L = 4.25$, Gr* = 0.07). The predictions (lines) are with G$_N^0$ = 0.22 MPa, and $\tau_e = 0.39$ s for PS390K and $\tau_e = 0.44$ s for PS50K, PS100K and the blends. The terminal relaxation of the high molar mass component in blend BL1 is via CR (disentanglement). The terminal relaxation of the high molar mass component in BL2 is partly via reptation in fat tube (the shorter chains) and partly via disentanglement. The high molar mass component in blend BL3 relaxes by reptation in the thin tube, except for the small fraction with $M > 780$ kg/mol, which relaxes via disentanglement.

We next consider PB bimodal blends from Struglinski and Graessley [61] (Figs. 16 and 17) and Rubinstein and Colby [62] (Fig. 18) which have been influential in developing theories for relaxation in bimodal blends, but which occupy a relatively small area in the Viovy diagram. These blends have comparatively large $\tilde{Z}_L$ (long chains remain well entangled after the terminal relaxation of the short component) and small Gr* ensuring the terminal relaxation of the long component via reptation in the thin tube. Figure 16 shows the elastic and loss moduli for 41k/174k blends (Gr* = 0.0085) in log-log plot; the loss modulus is shown in a log-linear plot in Fig. 17. Figures 17(b) and 17(c) show the loss modulus in log-linear plot for the 41L/435L blends (Gr* = 0.02) and the 174L/435L blends (Gr* = 10^{-4}). Overall, our predictions capture the shifts in the modulus as a function of weight fraction of the long chains in all cases.
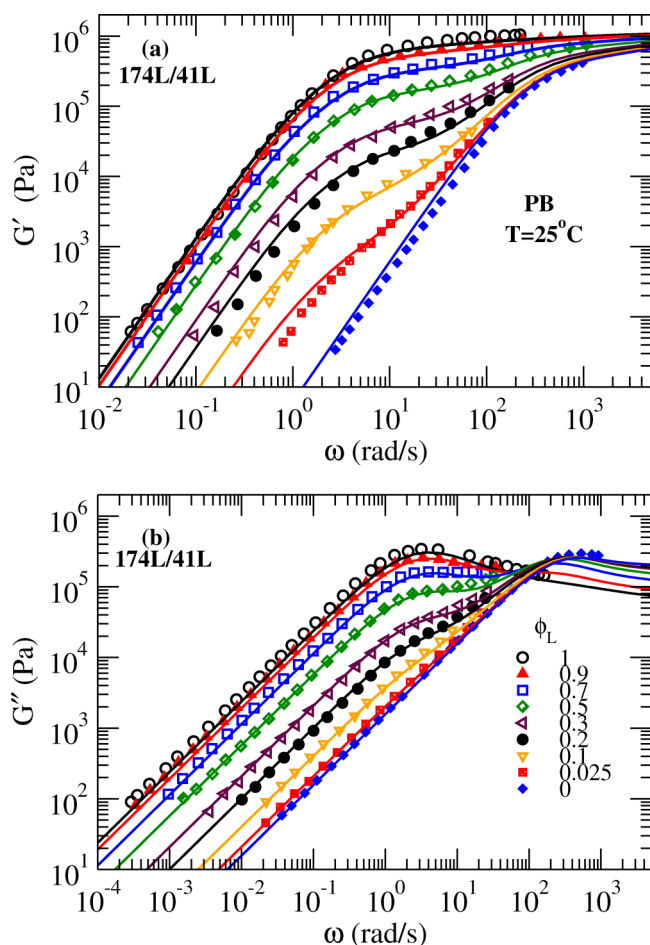
FIG. 16. Dynamic modulus G' and G'' for PB 41k/174k blends from Struglinski and Graessley [61] at the shown weight fractions along with predictions.

However, the experimental loss peak for 435L shows a wide high-frequency flank absent in our predictions. Figure 18 shows the loss modulus for blends of PB 355k and 71k ($\mathrm{Gr}^* = 1.5 \times 10^{-3}$) from [62] in the log-linear plot. This dataset captures both the reptation peaks from the short and the long components. While our predictions capture the shift in the reptation time of the short chains with concentration correctly, the height of the reptation peak for the short component in our model decreases faster than in the experiments as a function of the concentration of the short chains. Such differences are hardly visible on a log-log plot. It may be that capturing details down to the level of accuracy visible on a log-linear plot will require going beyond the mean field assumptions of this paper, toward an accounting for heterogeneity in the local environment of each chain.

Keeping the weight-fraction of the long chains fixed while varying the molar mass of the short components explores different values of Gr^* at a fixed $\tilde{Z}_L$ (i.e., vertical lines in the Viovy diagram of Fig. 9). In Figs. 19–22, we consider three such sets of blends with $\tilde{Z}_L = 0.72$, 3.4, 232, and 469.3 respectively.

Figure 19 shows the experimental data and predictions for blends of 0.5% PI 626K in various short matrix considered by Sawada *et al.* [18]. The long chains in these blends are
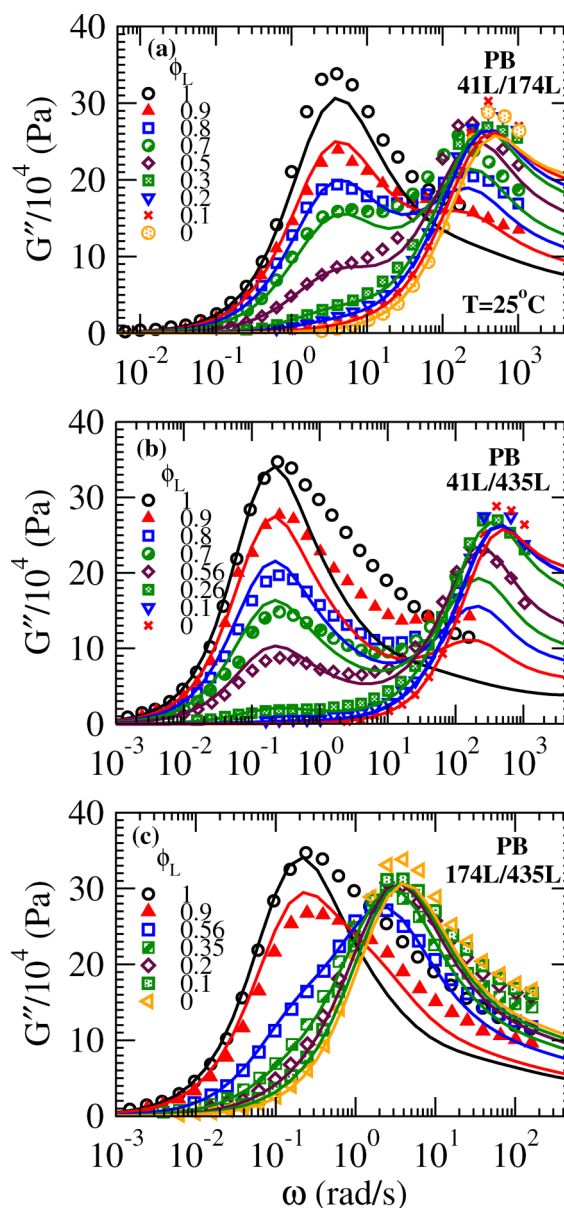

FIG. 17. Loss modulus G'' for PB 41k/174k, 41k/435k, and 174k/435k blends from Struglinski and Graessley [61] at the shown weight fractions along with predictions.
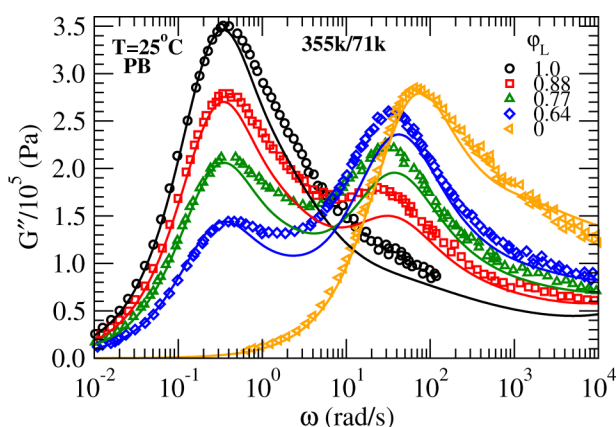

FIG. 18. Loss modulus G'' for PB 355k/71k blends from Rubinstein and Colby [62] at the shown weight fractions along with predictions.
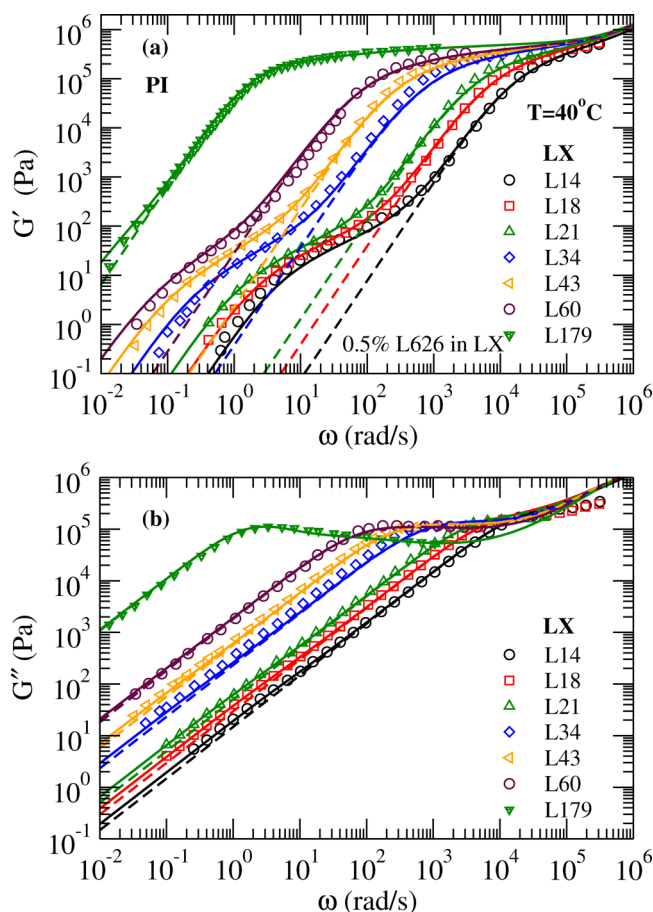
FIG. 19. Viscoelastic responses of 0.5% PI 626k in various short PI matrices from Sawada *et al.* [18] along with predictions.

FIG. 20. Viscoelastic responses for series of PS of different molar masses and 2% high molar mass F270 in short matrix from Montfort *et al.* [63]. The sample F270 is best described by $M_W = 2200$ kg/mol and PDI=2.0.

not self-entangled ($\tilde{Z}_L \simeq 0.72$). In making the predictions for the blends, we have used the values of τ_e fitted for the short majority components (Table II). The predictions for the viscoelastic responses for the pure short chains are shown with dashed lines, while those for the blends are shown as solid lines in Fig. 19. For the blends with L14k (Gr* = 7.7), L18k (Gr* = 3.9), L21k (Gr* = 1.9), L34k (Gr* = 0.35), and L43k (Gr* = 0.15), the long chains become unentangled in the supertube before they can relax by reptation, i.e., terminal relaxation is via a CR Rouse process. For the blends with 60K (Gr* = 4.9×10^{-2}) and 179k (Gr* = 1.2×10^{-3}), the terminal relaxation for the long chains is via reptation in the thin tube. Hence, our predictions are consistent with a small value for the critical Graessley parameter for transition between terminal relaxation via CR or via reptation.

Figure 20 shows experimental viscoelastic moduli (filled symbols) of 2% long PS F270 in various short PS matrix from Montfort *et al.* [63] along with the predictions (solid lines). Also shown are the experimental data and predictions, respectively, with open symbols and dashed lines for the single component polymers. The molar masses, polydispersity indices, and the entanglement times used for describing the single component polymers are shown in Table IV. The high molar mass samples F39 and F270 suggest $\tau_e = 1.9 \times 10^{-3}$ s at the reference temperature 160 °C ($\tau_e = 2.1 \times 10^{-4}$ s at 180 °C using the reported TTS shift factor). Using F39 as the reference sample and assuming that
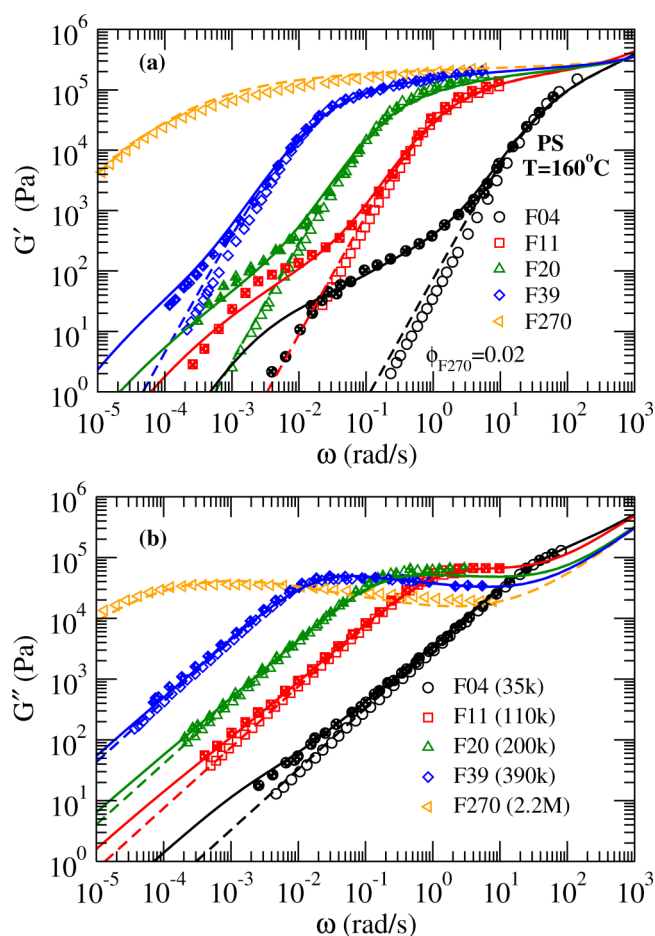
$\eta_0 \sim M_W^{3.4}$ holds for the high molar mass samples, we assign a molar mass of 2200 kg/mol for F270 instead of the reported 2700 kg/mol [63]. We also required a higher polydispersity (PDI = 2.0 instead of the reported 1.2) for this sample. Although such reassignment of both molar mass and PDI is not ideal, it appears to be justified from the rheology data of the pure sample. Predictions for the blends are made without further adjustment of the parameters, so the procedure appears robust. The lower molar mass samples are described with higher values of τ_e, possibly due to different glass transition temperatures from the chain-end effect.

We use the τ_e of the majority short component to describe the blends with 2% F270 ($\tilde{Z}_L = 3.4$) in Fig. 20. The long chains in the blend with F04 (Gr* = 17.8) become unentangled in the supertube before they can access reptation. The delayed CR in the blend with F11 results in terminal relaxation by reptation in thin tube for the chains with $M < 6 \times 10^2$ kg/mol (occupying 13 wt. % of F270). The longer chains in F270 become unentangled before they can relax via reptation. With further delay in CR in the blend with F20, this crossover molar mass is pushed to 6000 kg/mol and 95 wt. % of F270 relax by reptation in thin tube. The CR from the short component relaxation is slow enough in the blend with F39 matrix such that the terminal relaxation is entirely by reptation in thin tube for the long F270 component.
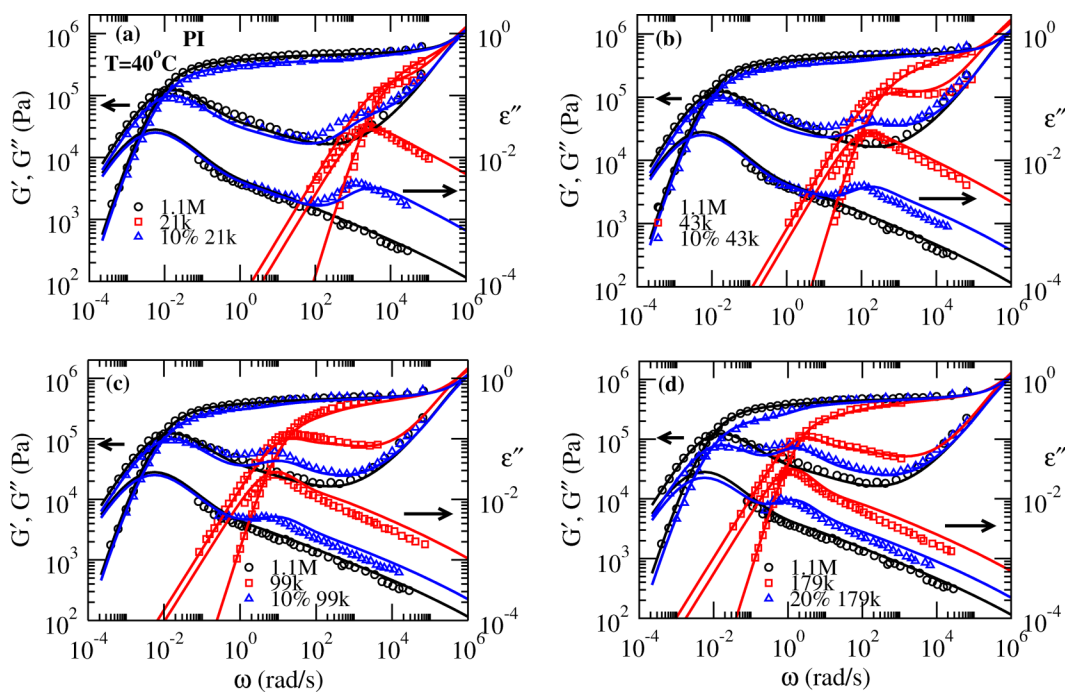
FIG. 21. Viscoelastic and dielectric responses for PI blends with (a) 10% 21k, (b) 10% 43k, (c) 10% 99k, and (d) 20% 179k in 1.1M matrix from Matsumiya *et al.* [46] along with predictions. $\mu''/10$ is used for predictions for the dielectric loss ϵ''.
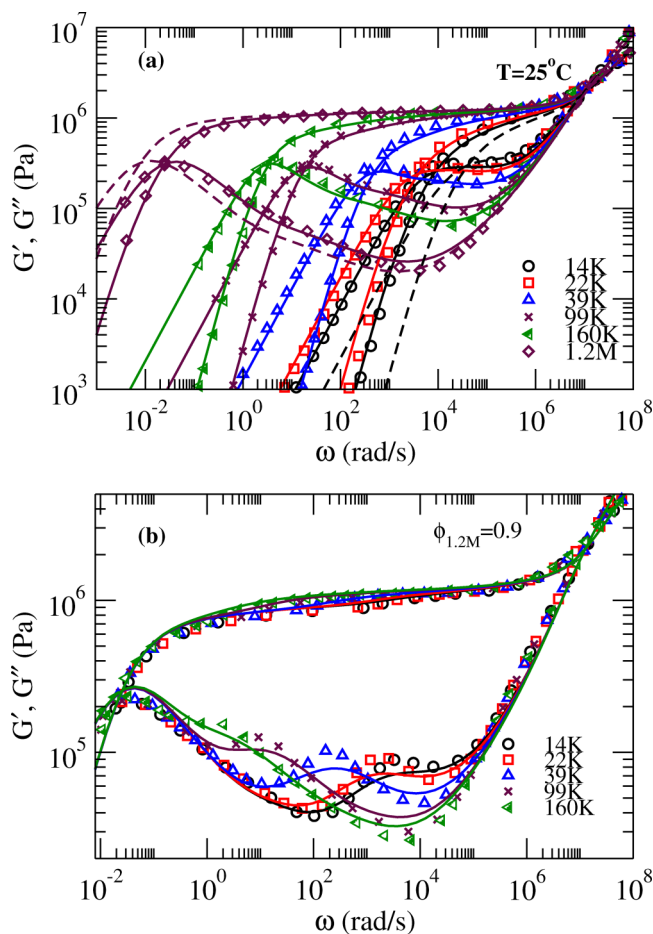

FIG. 22. (a) Viscoelastic responses and predictions for a series of PB from Liu *et al.* [64]. The predictions require significantly lower molar mass for the 1.2M sample and higher molar mass for the 14k sample. Predictions with reported molar masses are shown with dashed lines. (b) Viscoelastic responses of 10% PB 1.2M in various short PB matrices from Liu *et al.* [64] along with predictions.

In Fig. 21, we show experimental data for mechanical and dielectric relaxation from Matsumiya *et al.* [46] along with predictions from our model for PI 21k, 43k, 99k, 179k, 1.1M and blends with a minority of short chains in the 1.1M matrix at the shown weight fractions. The molecular characteristics and the values of τ_e used to make the predictions for the pure samples are shown in Table II. For the blends, the τ_e for the majority component 1.1M gives good agreement with the data. The long chains in the blends reptate in the thin tube. The first three blends (10% short chains) have $\tilde{Z}_L = 232$ and the Graessley number varies between $Gr^* = 3.4$ (blends with 21k) and $Gr^* = 0.016$ (blends with 99k). The blend with 179k has $\tilde{Z}_L = 206$ and $Gr^* = 0.002$. The large Z_L and comparatively small Gr^* ensure thin tube reptation for the long chains. However, the real interest here lies in the relaxation of short chains in the majority long chain matrix. The predictions capture the peak heights and positions of G'', and the peak heights of ϵ'' from the relaxation of the short chains and for the long chains in the blends correctly. We note that for the short chains in the blends, the relaxation times of $\mu(t)$ and rheological relaxation times are

TABLE IV. Molar mass, PDI, and entanglement time used in modeling for PS from Montfort *et al.* [63].

Label	M_W (kg/mol)	PDI	τ_e at 160 °C (10^{-3} s)
F04	35	1.06	3.5
F11	110	1.05	3.5
F20	200	1.06	2.0
F39	390	1.1	1.9
F270	2200	2.0	1.9
	(2700)	(1.2)	

similar, both being similar to the dielectric relaxation time of the pure short chains. This is because CR effects (which accelerate rheological relaxation) are suppressed in the blends. In contrast, the rheological relaxation time of pure short chains is faster, since this is accelerated by CR. For smaller molar masses of the short component [Figs. 21(a) and 21(b)], the experimental ϵ'' shows that the short component peak moves to lower frequencies in the blend compared to pure short components. This feature is not captured by μ'' in our predictions. We believe this may be because, for short chains, fluctuations of the chain ends about the tube axis [37] make a significant contribution to the dielectric relaxation. These end fluctuations become suppressed in a long matrix compared to pure short component and shift the dielectric peak to lower frequencies.

Figure 22(a) shows the experimental viscoelastic responses and the predictions for a series of PB considered by Liu *et al.* [64]. The responses for the samples 22K ($M_W = 22.8$ kg/mol, PDI $= 1.05$), 39K ($M_W = 38.6$ kg/mol, PDI $= 1.03$), 99K ($M_W = 98.8$ kg/mol, PDI $= 1.03$), and 160K ($M_W = 163$ kg/mol, PDI=1.01) are well described with $\tau_e = 2.5 \times 10^{-7}$ s. A significantly higher molar mass (19 kg/mol) compared to the reported $M_W = 13.2$ kg/mol is required to describe the lowest molar mass sample 14K (PDI=1.05). Similarly, a lower molar mass of 850 kg/mol compared to the reported 1240 kg/mol is required to describe the highest molar mass sample 1.2M (PDI $= 1.13$). The predictions with the reported molar masses for these two samples are shown with dashed lines in Fig. 22(a).

Figure 22(b) shows the viscoelastic responses of 10 wt. % of the short polymers in the long 1.2M matrix [64], which are again aimed at discerning the relaxation of short chains in a majority long chain matrix (the so-called "probe rheology"). As with the predictions for the single components samples, we use $M_W = 850$ kg/mol for the matrix polymer ($\tilde{Z}_L = 469$). The Graessley number Gr* for the blends varies between 2.5×10^{-4} (for blends with 160K) and 0.32 (for blends with 14K). The large $\tilde{Z}_L$ and not too large Gr* ensure that the terminal relaxation of the long component in all the blends is via reptation in the thin tube. The predictions correctly capture the frequencies of the local maximum in the G'' from the terminal relaxation of the short components. Again, the relaxation of the short components in the blends is slower as compared to the pure short chains (the latter being accelerated by CR).

E. Polydisperse polymers

In our approach, polydispersity is included from the beginning and all the results shown so far already include mild polydispersity even for "monodisperse" components.

For large polydispersity, specifying only the first two moments of the molar mass distribution (i.e., M_N and M_W) may not be sufficient to characterize the distribution. For this reason, first we consider two artificially constructed polydisperse PS created by blending narrowly distributed samples by Wasserman and Graessley [65]. The weight fractions of the components were chosen to mimic smoothly varying broad distributions. The sample M1 was constructed by

mixing 0.1% 2.98k, 0.2% 5.57k, 0.4% 9.1k, 0.8% 19.6k, 3% 37.9k, 15% 96.4k, 26% 190k, 35.8% 355k, 14% 706k, 3.9% 1.09M, and 8% 2.89M. The sample M2 was constructed by adding ~1.2% higher molar mass component (3.84M and 4.48M occupying 0.7% and 0.3% of the total material in M2) in a solution of M1. Thus, the two polymers have nearly identical M_N, but the higher moments of M2 are significantly larger than those of M1. In our numerical calculations, we assume that the reported molar masses of the components refer to their weight averaged molar masses and use a PDI=1.01 for each component. Figure 23(a) shows the viscoelastic responses of these two samples at a reference temperature of 150 °C along with predictions from our model using $\tau_e = 8.58 \times 10^{-3}$ s. The predictions correctly capture the slight increase in the viscous response and the more significant increase in the elastic response for M2 at low frequencies, as compared to the responses of M1. For both the samples, the first three components are unentangled. The remaining components show enhanced CLF due to relaxation of shorter components, but the final reptation for all these components is in the thin tube. This possibility of enhanced CLF in a fatter tube, but with reptation taking place along the thinner tube was discussed for binary blends in [13] and [14],
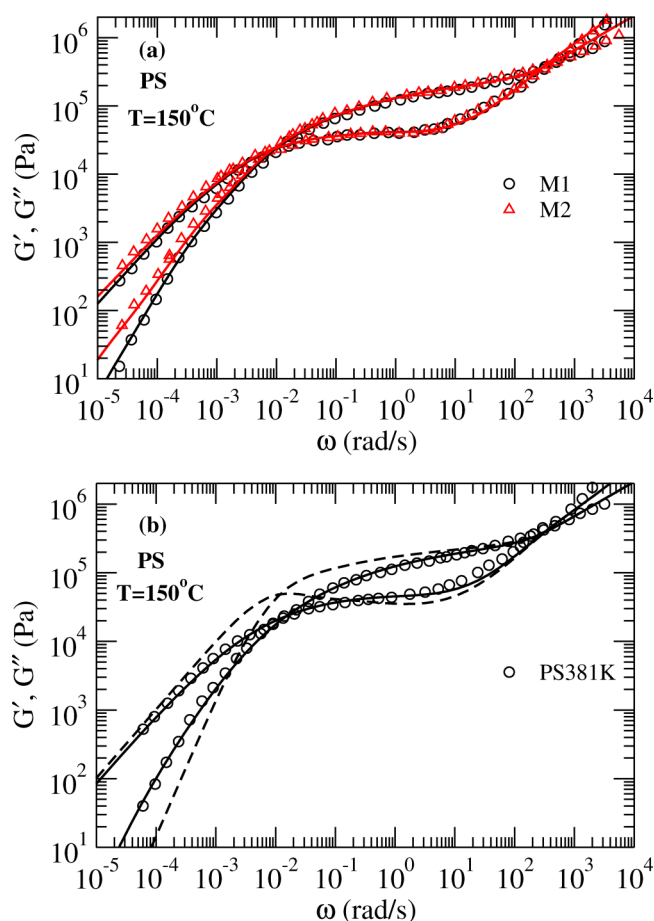
FIG. 23. (a) Dynamic modulus master curves at 150 °C for two multicomponent PS blends M1 and M2 from Wasserman and Graessley [65] along with predictions. (b) Results from a commercial PS with PDI=1.87 from the same reference. The solid lines are predictions based on the reported polydispersity, and the dashed lines are predictions with PDI=1.03 keeping M_W fixed.
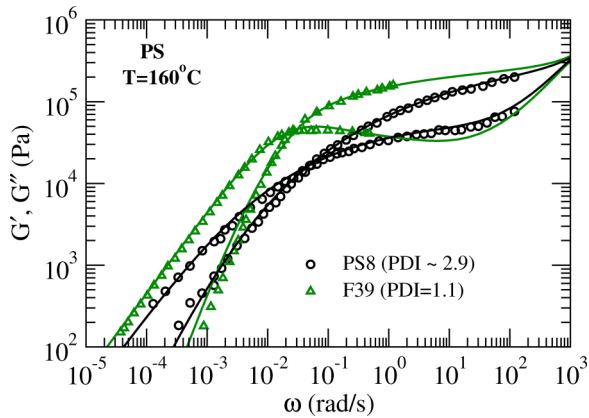
FIG. 24. Dynamic responses of a polydisperse sample PS8 from Montfort *et al.* [66] and a comparatively narrow dispersity sample F39 from Montfort *et al.* [63].

in the context of datasets such as those in Figs. 10 and 11. In the present model, it means that ϕ_{eq} is less than one (and a_{eq} larger than the thin tube) allowing freedom for enhanced CLF. Yet, Ψ_{min} remains close to 1 (i.e., chain transport is faster along the thin tube and $a_T = a_0$). Equation (27) indicates how these two factors combine to give an enhanced CLF rate.

Figure 23(b) shows the viscoelastic responses and predictions for a commercial PS ($M_W = 321\,\text{kg/mol}$, PDI = 1.87) from [65]. For these predictions, we assume that a log-normal distribution provides sufficiently accurate description of the molar mass distribution. The figure also shows predictions for a hypothetical polymer with the same weight averaged molar mass, but with narrow polydispersity (PDI = 1.03). In both cases, the reptation relaxation of the entangled chains is in the thin tube. The higher polydispersity in this case smoothens the reptation peak in G'' and reduces the modulus at the reptation peak compared to narrowly distributed sample.

Figure 24 shows the experimental viscoelastic responses of a high polydispersity sample PS8 from Montfort *et al.* [66] and a low polydispersity sample F39 ($M_W = 390k$, PDI=1.1) from Montfort *et al.* [63] together with theoretical predictions. The peak area in the GPC data of PS8 is well described by a log-normal distribution with $M_W = 390k$ and PDI=2.9. However, the log-normal distribution was found to overestimate the high molar mass tail. Thus, the true M_W of PS8 is lower than 390k. We model PS8 with a log-normal distribution with an exponential cutoff with a characteristic molar mass $3.5 \times 10^6\,\text{g/mol}$. The predictions in Fig. 24 use $\tau_e = 2 \times 10^{-3}\,\text{s}$ corresponding to the reference temperature of $160\,^\circ\text{C}$.

IV. SUMMARY AND OUTLOOK

The algorithm presented in this paper can be considered making use of ideas developed in earlier papers [13,14,31] for rheology and chain dynamics in binary polymer blends, but generalizing these to include the multiple CR times for fully polydisperse systems. Although the form of the algorithm is consistent with those earlier papers, we have allowed experimental data to guide choices of parameters, where appropriate. We have also included suitable crossovers to describe early time relaxation and the transition between entangled and unentangled motion. The algorithm has been tested against linear stress and dielectric relaxation data for a very broad range of monodisperse, bidisperse, and polydisperse polymer melts. We view the key elements and developments in the algorithm to be as follows:

- A nested tube structure based broadly on the dynamic dilution picture (see Fig. 1). In addition to the commonly used thin tube (no dilution), fat tube (full dilution), and supertube (indicating stress relaxation by CR), we added two more: an optimal tube for the fastest reptation (along-tube) motion, in Sec. II E; and an "equilibration" tube (the largest available tube for reptation or CLF), in Sec. II D.
- We reject Eq. (6) for stress relaxation (commonly used in branched polymer theories, including our own [25]) in favor of Eqs. (2), (4), and (5), which are closer to the double reptation [12] picture and to the expression used by Likhtman and McLeish [9] for monodisperse material.
- CR is modeled as an immediate drop in the supertube fraction ϕ_{ST} followed by power-law decay (see Fig. 2 and discussion in Sec. II C). This, combined with the equation used for stress relaxation, is essential for reproducing differences in dielectric and stress relaxation times, and change in relaxation time of short chains when embedded in long chain matrix (see Appendix B).
- CLF proceeds at a rate determined by the optimal tube for the fastest along-tube motion, but to a depth permitted by local equilibration from CR (i.e., CLF in a "fat" tube via motion along a thinner tube [13,14]), as detailed in Sec. II F.
- We also reexamined the criterion used for crossover from CLF to reptation relaxation, in Sec. II G. Here we found that the criterion used in some earlier models (BoB [25] and Hierarchical [24]) overestimated both relaxation due to CLF and the extent to which CLF accelerates terminal reptation.

The excellent comparison with experimental data suggests that this algorithm can be useful in making predictions for linear rheology of a substantial range of polydisperse polymer melts.

Nevertheless, it will be apparent even from the brief summary above that the model developed is, in several respects, not compatible with our previous algorithm to determine linear rheology of branched polymers (the BoB model [25]) or with the previous work upon which that algorithm builds. Although designed for branched polymers, the BoB model can be used to predict rheology of broadly polydisperse linear polymers, but will often require a different parameterization to that used in this paper. Especially for some of the binary blend data used in the present work, the BoB model will not work. There is a clear need to revisit theories for branched polymer relaxation in light of the more recent understanding of interaction between CR, CLF, and reptation emerging from studies of binary blends.

The computer source code used in generating the predictions in this paper, executable and documentation are available for download at https://github.com/chinmaydaslds/LP2R.

AUTHOR DECLARATIONS

Conflict of Interest

The authors have no conflicts to disclose.

DATA AVAILABILITY

The data that support the findings of this study are openly available in https://github.com/chinmaydaslds/LP2R, Ref. 67.

APPENDIX A: ON THE OBSERVATION OF DISTINCT a_{ST} AND a_{eq} IN SLIP-SPRING SIMULATIONS

Our claim that we need to keep track separately of two tubes, the "supertube" a_{ST} and "equilibration tube" a_{eq} (with associated volume fractions ϕ_{ST} and ϕ_{eq}) are not intuitively obvious. Typically, in tube theories, it has been considered that these two tubes are equal. As noted above, one reason for claiming that these two tubes are not equal lies in observations from the slip-spring simulations of [14] and [31]. Because those papers did not explicitly draw attention to this difference, in this appendix, we highlight the relevant features of those simulations and their analysis.

Both [14] and [31] make use of an effective friction constant per monomer (or simulation bead) arising from CR

Rouse motion, which is (for a slow CR process)

$$\zeta_{CR} = \frac{2k_B T}{b^2 N_e^2 \alpha_{CR}^2} \tau_{CR}, \tag{A1}$$

where τ_{CR} is the mean hop time of a single time scale CR process. The parameter α_{CR} was found to equal 1.2 by measurement of diffusion of chains in a slip-spring model where reptation was suppressed [31]. Hence, a chain subsection of N monomers has a CR Rouse time of

$$\tau_{RCR} = \frac{N^2 b^2 \zeta_{CR}}{3\pi^2 k_B T} = \frac{2N^2}{3\pi^2 \alpha_{CR}^2 N_e^2} \tau_{CR}. \tag{A2}$$

This can be used to obtain an effective supertube volume fraction (for diffusion and stress relation) by setting $\phi_{ST} = N_e/N$ and $\tau_{RCR} = t$ to give

$$\phi_{ST}(t) = \sqrt{\frac{2}{3\pi^2 \alpha_{CR}^2} \frac{\tau_{CR}}{t}}. \tag{A3}$$

The fact that this is not simply $\phi_{ST}(t) = \sqrt{\tau_{CR}/t}$ is one reason why we propose a drop in ϕ_{ST} in Sec. II C, since the asymptotic $\phi_{ST}(t)$ is smaller than expected.

Read *et al.* [14] also examines the effect of CR on the CLF process in the slip-spring model. One qualitative observation (see Fig. 3 of [14]) is that enhanced CLF in wider tubes does not occur significantly until after the typical CR time scale τ_{CR}. There, thus, is no evidence of a sudden jump at τ_{CR} in the widening tube for CLF (in contrast to ϕ_{ST}) but instead a smooth onset of enhanced CLF. This, then, is already a clue that a separate tube diameter will be required. Equation
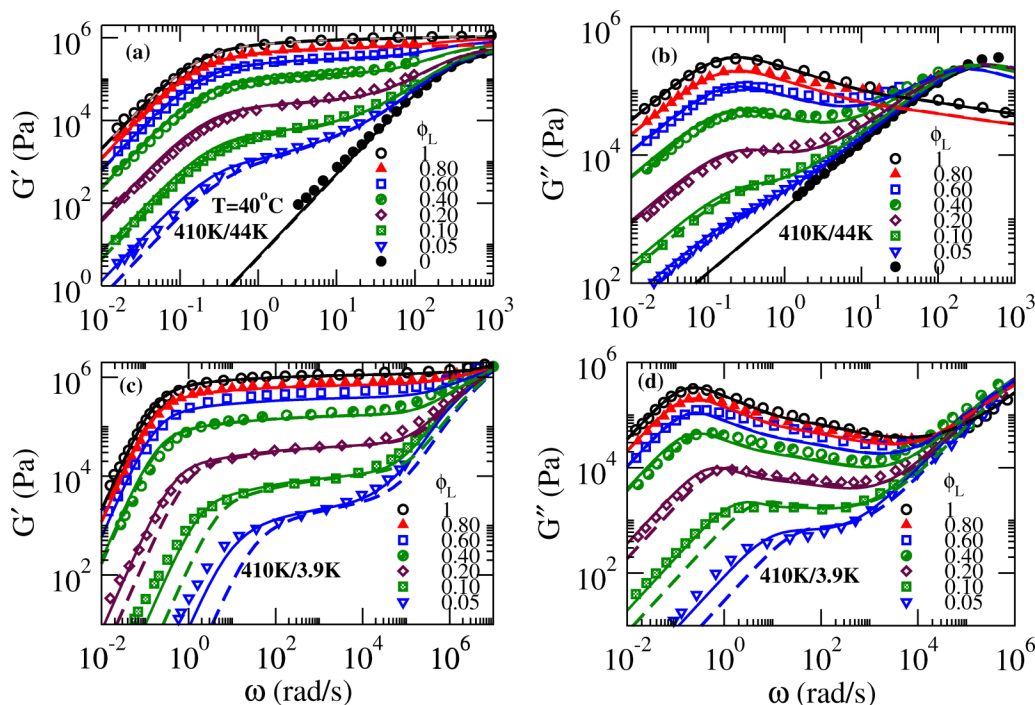
FIG. 25. Influence of A_{eq} on relaxation in binary blends: PB blend experimental data from Wang *et al.* [16], the solid lines are predictions with $A_{eq} = 2$ and the dashed lines are predictions with $A_{eq} = 1$.

(5) of [14] specifies the effective equilibration ϕ_{eq} used to model the data in their Fig. 3. Asymptotically, in the limit of slow CR and dilute long chains, this gives at long time

$$\phi_{eq} = \sqrt{\frac{\tau_{hop}}{t}} = \sqrt{\frac{2c_\phi}{\alpha_{CR}^2}\frac{\tau_{CR}}{t}}, \tag{A4}$$

where the hop time was specified as

$$\tau_{hop} = \frac{c_\phi N_e^2 b^2 \zeta_{CR}}{k_B T}, \tag{A5}$$

and the parameter c_ϕ was in fact set equal to 1 to model the data.

Comparing Eqs. (A3) and (A4) indicates that, at least for successful modeling of the slip-spring simulations, ϕ_{ST} (which governs diffusion and stress relaxation from CR processes) and ϕ_{eq} (which governs the tube in which CLF can occur) are not the same. Indeed, typically ϕ_{eq} is larger than ϕ_{ST} at any given time, and correspondingly a_{eq} is smaller than a_{ST}. One consequence in [14] can be observed in their Fig. 6 for the modified Viovy diagram. The boundary between regions 3 and 4 (a competition between reptation in thin and fat tubes, related to ϕ_{ST}) is shifted downwards in the diagram, indicating that diffusion along the fat tube is faster than might be expected. However, the boundary between regions 3c and 3b (a competition between CLF in the fat tube or thinner tubes, related to ϕ_{eq}) is not correspondingly shifted downwards. This is another indication of ϕ_{ST} being faster than ϕ_{eq}.

In Fig. 25, we illustrate the effect of considering a_{eq} different from a_{ST} for two set of PB blends from Wang *et al.* [16]. The dashed lines are predictions with $A_{eq} = 1$ (i.e. $a_{eq} = a_{ST}$), while the solid lines are with $A_{eq} = 2$. All other parameters are the same as in the predictions for Fig. 13. In logarithmic scale, the effect of A_{eq} is visible only when the reptation time of the two components is sufficiently well-separated such that the long chains undergo CLF in the fat tube for a substantial portion of its relaxation before reptation (Z_S is small), and there is a large change in a_{ST} from the relaxation of the short chains (ϕ_L is small). For the 410K/44K blends (panels a and b), the relaxation spectra between the two choices of A_{eq} are slightly different for the 5% and 10% blends. For higher ϕ_L, the two curves are indistinguishable in the figure. The difference is more prominent for the 410K/3.9K blends (panels c and d), where the difference is visible up to $\phi_L = 0.2$.

APPENDIX B: ON DOUBLE REPTATION AND THE EXPRESSION FOR STRESS RELAXATION

In this paper, we make use of Eqs. (2), (4), and (5) to calculate the stress relaxation function, contrasting this with the equation commonly used in branched polymer tube theories, Eq. (6). Here, we briefly discuss the difference between these expressions when applied in the simple double-reptation [12] limit for binary blends. We assume a blend with fraction ϕ_S short chains with bare reptation time τ_S, and fraction $\phi_L = 1 - \phi_S$ long chains with bare reptation time τ_L. Then, a simplified double reptation picture [5] can be obtained by assuming both $\phi(t)$ and $\phi_{ST}(t)$ obey

$$\phi(t) = \phi_{ST}(t) = \begin{cases} 1 & t < \tau_S, \\ \phi_L & \tau_S < t < \tau_L, \\ 0 & t > \tau_L. \end{cases} \tag{B1}$$

With dilution exponent 1, this then gives, from Eqs. (4) and (5),

$$\mu(t) = R(t) = \phi_L \exp\left(-\frac{t}{\tau_L}\right) + \phi_S \exp\left(-\frac{t}{\tau_S}\right), \tag{B2}$$

and so, using Eq. (2)

$$\frac{G(t)}{G_N^0} = \phi_L^2 \exp\left(-\frac{2t}{\tau_L}\right) + \phi_S^2 \exp\left(-\frac{2t}{\tau_S}\right)$$
$$+ 2\phi_L\phi_S \exp\left(-\frac{t}{\tau_L} - \frac{t}{\tau_S}\right). \tag{B3}$$

although greatly simplified, this has features that are broadly consistent with experimental observations. These can be observed by considering different limits as follows:

1. For pure long (or short) chains, e.g., $\phi_L = 1$, there is a factor of two difference between relaxation time of stress, $G(t)$, and dielectric response, $\mu(t)$. Such a difference can be observed in, for example, Fig. 5.
2. For pure short chains ($\phi_S = 1$), the stress relaxation time is obtained from the second term in Eq. (B3) and is $\tau_S/2$. In contrast, for short chains in a long chain matrix ($\phi_S \ll 1$ and $\tau_L \gg \tau_S$), the short-time stress relaxation is dominated by the last term in Eq. (B3), with relaxation time close to τ_S, which is also the dielectric relaxation time. Such observations are qualitatively clear, for example, in Figs. 21(c) and 21(d).

In Eq. (B3), these two predictions arise due to a combination of using Eqs. (2), (4), and (5) for the stress relaxation, and also having a step drop in ϕ_{ST} giving a substantial amount of CR at the time scale of relaxation of the entangling chains. Although we go beyond the double reptation approximation, we retain these features in the theoretical development in the main body of the paper.

In contrast, using Eq. (6) with Eq. (B1) gives

$$\frac{G(t)}{G_N^0} = \phi_L^2 \exp\left(-\frac{t}{\tau_L}\right) + (1 - \phi_L^2)\exp\left(-\frac{t}{\tau_S}\right). \tag{B4}$$

This gives neither the factor of two difference between stress and dielectric relaxation time for pure chains nor the difference in stress relaxation peak for short chains in long chain matrix. We believe it impossible to reproduce these key experimental observations using Eq. (6) for stress relaxation.
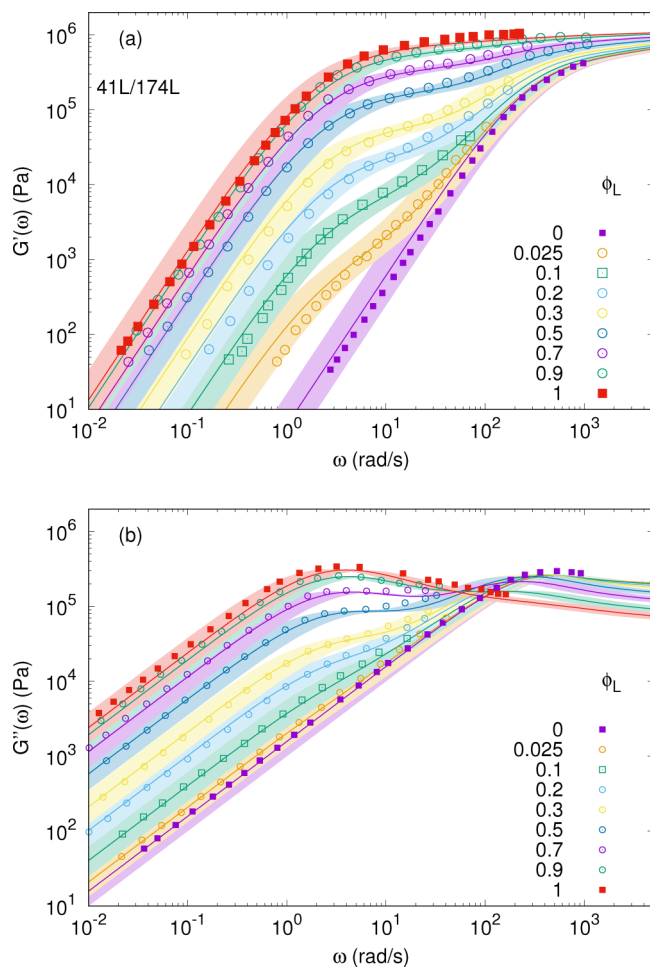
FIG. 26. One PB blend series from Struglinski and Graessley [61] with confidence bands showing the prediction with 15% uncertainty in the molar mass.

APPENDIX C: MODEL PARAMETERS AND EXPERIMENTAL DATA WITH SYSTEMATIC ERRORS

In an idealized scenario, experimental data are of use for a model such as ours in three distinct ways: first, the model parameters can be fitted with a subset of data from *fully specified* samples. Second, a separate set of *fully specified* samples serve to validate the model. Third, the model can estimate experimental parameters for results from a *partially specified* experiment. To avoid circularity, these three sets should ideally be separate. Ideally, the fitting procedure for parameters should consider experimental uncertainties to yield a parameter range and predictions should give confidence bands.

The above procedure is feasible for experiments where random errors dominate the results. Unfortunately, the main uncertainty in polymer rheology data is dominated by systematic errors in polymer characterization (molar mass distribution, glass transition temperature, etc.). Considering the scatter in the zero-shear viscosity shown in Fig. 3, and for now attributing the observed scatter in the data only to the uncertainty in the molar mass determination, in Fig. 26 we replot our results on PB 174K/41K blends from Struglinski and Graessley [61] assuming that the molar masses of the two components can be $\pm 15\%$ different from the specified molar masses (a reasonable confidence interval for GPC).

The uncertainty in the polymer translates to confidence bands in our predictions.

As can be seen in Fig. 3, the confidence bands for the different concentrations overlap with each other considerably. However, since the experimental errors are mostly systematic, the different concentration data will most likely share a correlated systematic error (e.g., in the long component molar mass is higher, then all the predictions are pushed toward longer terminal relaxation time). This feature of correlated error is not well represented by simple confidence bands. Further, for an individual sample, a systematic error in molar mass can be compensated by adjusting other model parameters. Across a wider range of samples, this interplay between potential characterization errors and potential errors in model parameters results in a degree of circularity that tends to break the idealized scenario presented at the start of this appendix.

Hence, pragmatically, we present our predictions as lines rather than confidence bands in our plots. In our model validation/prediction, we have reassigned molar masses of the parent components where necessary. Similarly, for a single concentration, the entire frequency response shares the same glass-transition temperature (T_g). Where necessary, we have used separate τ_e to describe individual blends with the constraint that the blends must have T_g that lies between the two T_g of the parent components: i.e., τ_e of the blends lie between the τ_e required for the parent components and vary systematically depending on the concentration.

APPENDIX D: ON NUMERICAL VALUE OF A_ζ

For the slip-spring simulations, Read *et al.* [14] assigned a value of $A_\zeta = 0.047$ based on a measurement of the diffusion of chains with constraints having a well-defined exponential distribution of CR times with time constant τ_{CR}. In this appendix, we discuss the reason that their estimate of A_ζ was so different from the one used in this paper. Slip-springs are just an idealized model, and there is no particular reason to expect that CR in real polymers follows exactly the same path as in slip-springs (in particular, a real entanglement could be a collective effect of interactions with multiple chains). So, the real A_ζ could easily be different from the slip-spring simulation value.
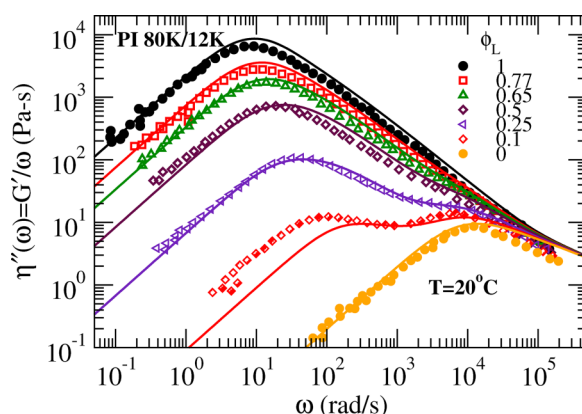

FIG. 27. Imaginary part of the complex viscosity η'' for PI 80K/12K blends from Malo de Molina *et al.* [52] along with predictions.

The parameter A_ζ is not directly accessible from the experiments. Read *et al.* [14] provided a formula that can describe the terminal relaxation time of the long chains in a bimodal blend based on the number of entanglements of the components, volume fraction, and the relaxation time of the short chains. Malo de Molina *et al.* [52] used this formula to show that the terminal time of the long chains in a 80K/12K blend can be described by the form of Read *et al.* [14]. The agreement for the terminal time of the long chains at high volume fraction of long chains in itself does not *prove* that real chains require $A_\zeta = 0.047$. In fact, the interpolation form for the friction is so arranged is to make it rather insensitive of A_ζ at high ϕ_L. Malo de Molina *et al.* presented their data in terms of real and imaginary viscosity components and the relaxation time was accessed from the peak in the imaginary viscosity. In Fig. 27, we show that our current model detailed model with $A_\zeta = 1.25$ describes the terminal time of the long chains in the experiments of Malo de Molina *et al.* equally well (and also describes the full frequency spectra). The predictions use $\tau_e = 1.9 \times 10^{-5}$ s.

To investigate the effect of CLF, we show the time evolution of $\phi(t)$, $\phi_{ST}(t)$, $\mu(t)$, and $R(t)$ in Fig. 28 from a separate calculation for the 10% blend where we ignored the small polydispersity to aid in visualization.

The first drop in ϕ_{ST} (orange symbols) is at τ_e. It then follows (and in the graph completely overlaps) the relaxation of $\phi(t)$ due to CLF until the terminal relaxation at $\tau_{d,s} \sim 1.7 \times 10^{-4}$ s. At this point, $\phi(t)$ drops to just below 0.1 as the short chains reptate. There is a corresponding drop in ϕ_{ST} from a value of 0.44 to a value of 0.35 followed by supertube relaxation until 4×10^{-3} s. We note here that a substantial part of the relaxation of ϕ_{ST} (from a value of 1 down to a value of 0.44) is provided by CLF and then the last part (from 0.44 to 0.35) by the δ_{CR} parameter, which we relate to an effective A_ζ.

An approximate description for the above system (commensurate with the previous analysis of Read *et al.* [14] based on a single CR time scale) would be to hold value of $\phi_{ST} = 1$ until the terminal relaxation $\tau_{d,s}$ followed by a larger drop (from 1 to 0.35) to give the same $\phi_{ST}(t)$, or equivalently $R(t)$ in the supertube relaxation region. In this particular case,
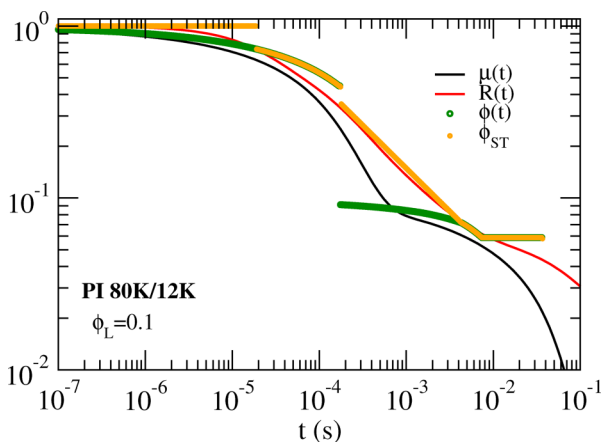
assigning a single CR time at $\tau_{d,s}$ will lead to a much larger value of δ_{CR} corresponding to a value of A_ζ that is about a factor 7 smaller than 1.25 used in our current model.

Thus, proper incorporation of CLF explains partly the reason of the different values of A_ζ required in our model and in model based on slip-spring simulations. In the particular example of Molina *et al.* [52], the lack of CLF in a simplified model accounts for a factor 7 difference in the value of A_ζ compared to the current more detailed model. This still leaves a factor of 3.8 difference between the two models. However, the parameter A_ζ does not appear in isolation, but rather is combined with multiple other parameters to predict the observed relaxation spectra. These other parameters do not have similar physical meaning to connect between the two theories directly. In general, the experimental systems where the value of δ_{CR} or A_ζ is important are typically ones where the short chains are a relatively short (in terms of the number of entanglements) and where CLF effects are large. As is evident in this work, we describe a wide range of data with the current parameterization.

APPENDIX E: CALCULATION OF THE DYNAMIC MODULI

The dynamic moduli are calculated from the decay of Φ and Φ_{ST} as

$$\frac{G^*(\omega)}{G_N^0} \equiv i\omega \int_0^\infty ds\, \mu(t)\, R(t) e^{-s(i\omega+s)} = \int_{\tau_k} d\tau_k \left(-\frac{d\phi}{d\tau_k}\right)$$
$$\times \int_{\tau_m} d\tau_m \left(-\frac{d\phi_{ST}^\alpha}{d\tau_m}\right)\left[\frac{\omega^2\tau_{km}^2}{1+\omega^2\tau_{km}^2} + i\frac{\omega\tau_{km}}{1+\omega^2\tau_{km}^2}\right].$$
$$(E1)$$

Here, $\tau_{km} \equiv \tau_k\tau_m/(\tau_k + \tau_m)$ and the integrals involving τ_k and τ_m are between zero and infinity. Since ϕ goes to zero at the final reptation time τ_d of the last surviving polymer, the first integral can be approximated as

$$\int_{\tau_k} d\tau_k \left(-\frac{d\phi}{d\tau_k}\right) \Rightarrow \sum_k^{\tau_k \leq \tau_d} [-\Delta\phi(\tau_k)]. \qquad (E2)$$

Taking account of the long-time power-law decay of Φ_{ST} beyond the terminal reptation time, we divide the second integral as a sum until τ_d where we accumulate values of Φ_{ST} at discrete time intervals and an integral as

$$\int_{\tau_m} d\tau_m \left(-\frac{d\phi_{ST}^\alpha}{d\tau_m}\right) \Rightarrow \left\{ \sum_m^{\tau_m \leq \tau_d} [-\Delta\phi_{ST}^\alpha(\tau_m)] \right.$$
$$\left. + \frac{\phi_{ST}^\alpha(\tau_d)\sqrt{\tau_d}}{2}\int_{\tau_d}^\infty d\tau_m \tau_m^{-3/2} \right\}. \quad (E3)$$

FIG. 28. Time evolution of $\mu(t)$, $R(t)$, $\phi(t)$, and $\phi_{ST}(t)$ for PI 10% 80K polymer in 12K matrix.

The resulting integrals in the complex modulus allow

closed form expressions as

$$
\begin{aligned}
\mathcal{I}' &\equiv \int_{\tau_d}^{\infty} d\tau_m \left(-\frac{d\phi_{ST}^{\alpha}}{d\tau_m} \right) \frac{\omega^2 \tau_{km}^2}{1 + \omega^2 \tau_{km}^2} \\
&= \frac{\phi_{ST}^{\alpha}(\tau_d)}{2} \omega^2 \tau_k^2 \int_1^{\infty} \frac{\sqrt{x}\,dx}{\omega^2 \tau_k^2 x^2 + (\tau_k/\tau_d + x)^2} \\
&\equiv \frac{\phi_{ST}^{\alpha}(\tau_d)}{2} \omega^2 \tau_k^2 \, \mathcal{I}_1\left(\frac{\tau_k}{\tau_d}, \omega^2 \tau_k^2 \right),
\end{aligned} \quad (E4)
$$

$$
\begin{aligned}
\mathcal{I}'' &\equiv \int_{\tau_d}^{\infty} d\tau_m \left(-\frac{d\phi_{ST}^{\alpha}}{d\tau_m} \right) \frac{\omega \tau_{km}}{1 + \omega^2 \tau_{km}^2} \\
&= \frac{\phi_{ST}^{\alpha}(\tau_d)}{2} \omega \tau_k \int_1^{\infty} \frac{dx}{\sqrt{x}} \frac{(\tau_k/\tau_d + x)}{\omega^2 \tau_k^2 x^2 + (\tau_k/\tau_d + x)^2} \\
&\equiv \frac{\phi_{ST}^{\alpha}(\tau_d)}{2} \omega \tau_k \, \mathcal{I}_2\left(\frac{\tau_k}{\tau_d}, \omega^2 \tau_k^2 \right).
\end{aligned} \quad (E5)
$$

For real positive $a \leq 1$ and real positive b, the integrations $\mathcal{I}_1(a, b)$ and $\mathcal{I}_2(a, b)$ result in

$$
\begin{aligned}
\mathcal{I}_1(a, b) &\equiv \int_1^{\infty} \frac{\sqrt{x}\,dx}{(a+x)^2 + bx^2} \\
&= \frac{1}{2\sqrt{2}\alpha\beta a} \left[\frac{\beta\gamma(1+\alpha)t_1}{b} - 2\sqrt{a}\,t_2 \right],
\end{aligned} \quad (E6)
$$

$$
\begin{aligned}
\mathcal{I}_2(a, b) &\equiv \int_1^{\infty} \frac{dx}{\sqrt{x}} \frac{(a+x)}{(a+x)^2 + bx^2} \\
&= \frac{1}{2\sqrt{2}\alpha\beta a} \left[-\gamma\beta t_1 - 2\sqrt{a}(1+\alpha)t_2 \right].
\end{aligned} \quad (E7)
$$

Here, $\alpha \equiv \sqrt{1+b}$, $\beta \equiv \sqrt{1+\alpha}$, $\gamma \equiv \sqrt{a(\alpha-1)}$, $\delta \equiv \sqrt{a(\alpha+1)}$, $t_1 \equiv \ln\left((a+\alpha+\sqrt{2}\gamma)/(a+\alpha-\sqrt{2}\gamma)\right)$, and $t_2 \equiv \tan^{-1}\left((2\sqrt{2}\alpha\delta)/(\delta^2+\gamma^2-2\alpha^2)\right)$.

REFERENCES

[1] de Gennes, P. G., "Reptation of a polymer chain in the presence of fixed obstacles," J. Chem. Phys. **55**, 572–579 (1971).
[2] Doi, M., and S. F. Edwards, "Dynamics of concentrated polymer systems. Part 1. Brownian motion in the equilibrium state," J. Chem. Soc. Faraday Trans. 2 **74**, 1789–1801 (1978).
[3] Doi, M., and S. F. Edwards, *The Theory of Polymer Dynamics* (Clarendon Press, Oxford, 1986).
[4] Rubinstein, M., and R. H. Colby, *Polymer Physics* (Oxford University Press, Oxford, 2003).
[5] Dealy, J. M., D. J. Read, and R. G. Larson, *Structure and Rheology of Molten Polymers* (Hanser, Munich, 2018).
[6] Doi, M., "Explanation for the 3.4-power law for viscosity of polymeric liquids on the basis of the tube model," J. Polym. Sci. Polym. Phys. Ed. **21**, 667–684 (1983).
[7] Milner, S. T., and T. C. B. McLeish, "Reptation and contour-length fluctuations in melts of linear polymers," Phys. Rev. Lett. **81**, 725–728 (1998).
[8] de Gennes, P. G., "Dynamics of entangled polymer solutions. I. The Rouse model," Macromolecules **9**, 587–593 (1976).
[9] Likhtman, A. E., and T. C. B. McLeish, "Quantitative theory for linear dynamics of linear entangled polymers," Macromolecules **35**, 6332–6343 (2002).
[10] Tuminello, W. H., "Molecular weight and molecular weight distribution from dynamic measurements of polymer melts," Polym. Eng. Sci. **26**, 1339–1347 (1986).
[11] Tsenoglou, C., "Molecular weight polydispersity effects on the viscoelasticity of entangled linear polymers," Macromolecules **24**, 1762–1767 (1991).
[12] des Cloizeaux, J., "Double reptation versus simple reptation in polymer melts," Europhys. Lett. **5**, 437–442 (1988).
[13] Read, D. J., K. Jagannathan, S. K. Sukumaran, and D. Auhl, "A full-chain constitutive model for bidisperse blends," J. Rheol. **56**, 823–873 (2012).
[14] Read, D. J., M. E. Shivokhin, and A. E. Likhtman, "Contour length fluctuations and constraint release in entangled polymers: Slip-spring simulations and their implications for binary blend rheology," J. Rheol. **64**, 1017–1036 (2018).
[15] Watanabe, H., and T. Kotaka, "Viscoelastic properties and relaxation mechanisms of binary blends of narrow molecular weight distribution polystyrenes," Macromolecules **17**, 2316–2325 (1984).
[16] Wang, S., S.-Q. Wang, A. Halasa, and W.-L. Hsu, "Relaxation dynamics in mixtures of long and short chains: Tube dilation and impeded curvilinear diffusion," Macromolecules **36**, 5355–5371 (2003).
[17] Park, S. J., and R. G. Larson, "Tube dilation and reptation in binary blends of monodisperse linear polymers," Macromolecules **37**, 597–604 (2004).
[18] Sawada, T., X. Qiao, and H. Watanabe, "Viscoelastic relaxation of linear polyisoprenes: Examination of constraint release mechanism," J. Soc. Rheol. Japan **35**, 11–20 (2007).
[19] van Ruymbeke, E., V. Shchetnikava, Y. Matsumiya, and H. Watanabe, "Dynamic dilution effect in binary blends of linear polymers with well-separated molecular weights," Macromolecules **47**, 7653–7665 (2014).
[20] Schieber, J. D., J. Neergaard, and S. Gupta, "A full-chain, temporary network model with sliplinks, chain-length fluctuations, chain connectivity and chain stretching," J. Rheol. **47**, 213–233 (2003).
[21] Likhtman, A. E., "Single-chain slip-link model of entangled polymers: Simultaneous description of neutron spin-echo, rheology, and diffusion," Macromolecules **38**, 6128–6139 (2005).
[22] Masubuchi, Y., J.-I. Takimoto, K. Koyama, G. Ianniruberto, G. Marrucci, and F. Greco, "Brownian simulations of a network of reptating primitive chains," J. Chem. Phys. **115**, 4387–4394 (2001).
[23] Uneyama, T., and Y. Masubuchi, "Multi-chain slip-spring model for entangled polymer dynamics," J. Chem. Phys. **137**, 154902 (2012).
[24] Larson, R. G., "Combinatorial rheology of branched polymer melts," Macromolecules **34**, 4556–4571 (2001).
[25] Das, C., N. J. Inkson, D. J. Read, M. A. Kelmanson, and T. C. B. McLeish, "Computational linear rheology of general branch-on-branch polymers," J. Rheol. **50**, 207–234 (2006).
[26] van Ruymbeke, E., C. Bailly, R. Keunings, and D. Vlassopoulos, "A general methodology to predict the linear rheology of branched polymers," Macromolecules **39**, 6248–6259 (2006).
[27] Doi, M., W. W. Graessley, E. Helfand, and D. S. Pearson, "Dynamics of polymers in polydisperse melts," Macromolecules **20**, 1900–1906 (1987).
[28] Viovy, J. L., M. Rubinstein, and R. H. Colby, "Constraint release in polymer melts: Tube reorganization versus tube dilation," Macromolecules **24**, 3587–3596 (1991).
[29] Park, S. J., and R. G. Larson, "Long-chain dynamics in binary blends of monodisperse linear polymers," J. Rheol. **50**, 21–39 (2006).

[30] Auhl, D., P. Chambon, T. C. B. McLeish, and D. J. Read, "Elongational flow of blends of long and short polymers: Effective stretch relaxation time," Phys. Rev. Lett. **103**, 136001 (2009).

[31] Shivokhin, M. E., D. J. Read, D. Kouloumasis, R. Kocen, F. Zhuge, C. Bailly, N. Hadjichristidis, and A. E. Likhtman, "Understanding effect of constraint release environment on end-to-end vector relaxation of linear polymer chains," Macromolecules **50**, 4501–4523 (2017).

[32] Marrucci, G., "Relaxation by reptation and tube enlargement: A model for polydisperse melts," J. Polym. Sci. Polym. Phys. Ed. **23**, 159–177 (1985).

[33] Blottiere, B., T. McLeish, A. Hakiki, R. Young, and S. Milner, "The rheology of bimodal blends of star polymer melts," Macromolecules **31**, 9295–9304 (1998).

[34] Milner, S., T. McLeish, R. Young, A. Hakiki, and J. Johnson, "Dynamic dilution, constraint-release, and star-linear blends," Macromolecules **31**, 9345–9353 (1998).

[35] Watanabe, H., O. Urakawa, and T. Kotaka, "Slow dielectric relaxation of entangled linear cis-polyisoprenes with asymmetrically inverted dipoles. 1. Bulk systems," Macromolecules **26**, 5073–5083 (1993).

[36] Watanabe, H., "Slow dynamics in homopolymer liquids," Polym. J. **41**, 929–950 (2009).

[37] Watanabe, H., Y. Matsumiya, and T. Inoue, "Dielectric and viscoelastic relaxation of highly entangled star polyisoprene: Quantitative test of tube dilation model," Macromolecules **35**, 2339–2357 (2002).

[38] Milner, S. T., and T. C. B. McLeish, "Parameter-free theory for stress relaxation in star polymer melts," Macromolecules **30**, 2157–2166 (1997).

[39] Shchetnikava, V., J. Slot, and E. van Ruymbeke, "Comparative analysis of different tube models for linear rheology of monodisperse linear entangled polymers," Polymers **11**, 754 (2019).

[40] Palade, L. I., V. Verney, and P. Attané, "Time-temperature superposition and linear viscoelasticity of polybutadienes," Macromolecules **28**, 7051–7057 (1995).

[41] Park, S. J., P. S. Desai, X. Chen, and R. G. Larson, "Universal relaxation behavior of entangled 1, 4-polybutadiene melts in the transition frequency region," Macromolecules **48**, 4122–4131 (2015).

[42] Auhl, D., J. Ramirez, A. E. Likhtmana, P. Chambon, and C. Fernyhough, "Linear and nonlinear shear flow behavior of monodisperse polyisoprene melts with a large range of molecular weights," J. Rheol. **52**, 801–835 (2008).

[43] Abdel-Goad, M., W. Pyckhout-Hintzen, S. Kahle, J. Allgaier, D. Richter, and L. J. Fetters, "Rheological properties of 1,4-polyisoprene over a large molecular weight range," Macromolecules **37**, 8135–8144 (2004).

[44] Watanabe, H., S. Ishida, Y. Matsumiya, and T. Inoue, "Viscoelastic and dielectric behavior of entangled blends of linear polyisoprenes having widely separated molecular weights: Test of tube dilation picture," Macromolecules **37**, 1937–1951 (2004).

[45] Watanabe, H., S. Ishida, Y. Matsumiya, and T. Inoue, "Test of full and partial tube dilation pictures in entangled blends of linear polyisoprenes," Macromolecules **37**, 6619–6631 (2004).

[46] Matsumiya, Y., K. Kumazawa, M. Nagao, O. Urakawa, and H. Watanabe, "Dielectric relaxation of monodisperse linear polyisoprene: Contribution of constraint release," Macromolecules **46**, 6067–6080 (2013).

[47] DÁgnillo, L., J. Soares, and A. Penlidis, "Round-robin experiment in high-temperature gel permeation chromatography," J. Polym. Sci. Part B: Polym. Phys. **40**, 905–921 (2002).

[48] Blanchard, L.-P., J. Hesse, and S. L. Malhotra, "Effect of molecular weight on glass transition by differential scanning calorimetry," Can. J. Chem. **52**, 3170–3175 (1974).

[49] Carella, J. M., W. W. Graessley, and L. J. Fetters, "Effects of chain microstructure on the viscoelastic properties of linear polymer melts: Polybutadienes and hydrogenated polybutadienes," Macromolecules **17**, 2775–2786 (1984).

[50] Klopffer, M. H., L. Bokobza, and L. Monnerie, "Effect of vinyl content on the viscoelastic properties of polybutadienes and polyisoprenes - monomeric friction coefficient," Polymer **39**, 3445–3449 (1998).

[51] Ferry, J. D., *Viscoelastic Properties of Polymers* (Wiley, New York, 1980).

[52] Malo de Molina, P., A. Alegría, J. Allgaier, M. Kruteva, I. Hoffmann, S. Prévost, M. Monkenbusch, D. Richter, A. Arbe, and J. Colmenero, "Tube dilation in isofrictional polymer blends based on polyisoprene with different topologies: Combination of dielectric and rheological spectroscopy, pulsed-field-gradient NMR, and neutron spin echo (NSE) techniques," Macromolecules **53**, 5919–5936 (2020).

[53] Roland, C. M., M. J. Schroeder, J. J. Fontanella, and K. L. Ngai, "Evolution of the dynamics in 1,4-polyisoprene from a nearly constant loss to a johari-goldstein β-relaxation to the α-relaxation," Macromolecules **37**, 2630–2635 (2004).

[54] Santangelo, P. G., and C. M. Roland, "Temperature dependence of mechanical and dielectric relaxation in cis-1,4-polyisoprene," Macromolecules **31**, 3715–3719 (1998).

[55] Mohamed, F., M. Flämig, M. Hofmann, L. Heymann, L. Willner, N. Fatkullin, N. Aksel, and E. A. Rössler, "Scaling analysis of the viscoelastic response of linear polymers," J. Chem. Phys. **149**, 044902 (2018).

[56] Schausberger, A., G. Schindlauer, and H. Janeschitz-Kriegl, "Linear elastico-viscous properties of molten standard polystyrenes. I. Presentation of complex moduli," Rheol Acta **24**, 220–227 (1985).

[57] Matsumiya, Y., A. Uno, and H. Watanabe, "Dielectric and viscoelastic investigation of segmental dynamics of polystyrene above glass transition temperature: Cooperative sequence length and relaxation mode distribution," Macromolecules **44**, 4355–4365 (2011).

[58] Baumgaertel, M., A. Schausberger, and H. H. Winter, "The relaxation of polymers with linear flexible chains of uniform length," Rheol Acta **29**, 400–408 (1990).

[59] Li, S. W., H. E. Park, and J. M. Dealy, "Evaluation of molecular linear viscoelastic models for polydisperse H polybutadienes," J. Rheol. **55**, 1341–1373 (2011).

[60] Nielsen, J. K., H. K. Rasmussen, O. Hassager, and G. H. McKinley, "Elongational viscosity of monodisperse and bidisperse polystyrene melts," J. Rheol. **50**, 453–476 (2006).

[61] Struglinski, M. J., and W. W. Graessley, "Effects of polydispersity on the linear viscoelastic properties of entangled polymers. 1. Experimental observations for binary mixtures of linear polybutadiene," Macromolecules **18**, 2630–2643 (1985).

[62] Rubinstein, M., and R. H. Colby, "Self-consistent theory of polydisperse entangled polymers: Linear viscoelasticity of binary blends," J. Chem. Phys. **89**, 5291–5306 (1988).

[63] Montfort, J. P., G. Martin, and P. Monge, "Effects of constraint release on the dynamics of entangled linear polymer melts," Macromolecules **17**, 1551–1560 (1984).

[64] Liu, C. Y., A. F. Halasa, R. Keunings, and C. Bailly, "Probe rheology: A simple method to test tube motion," Macromolecules **39**, 7415–7424 (2006).

[65] Wasserman, S. H., and W. W. Graessley, "Effects of polydispersity on linear viscoelasticity in entangled polymer melts," J. Rheol. **36**, 543–572 (1992).

[66] Montfort, J. P., G. Martin, J. Arman, and P. Monge, "Viscoelastic properties of high molecular weight polymers in the molten state. II. Influence of the molecular weight distribution on linear viscoelastic properties," Rheol Acta **18**, 623–628 (1979).

[67] Das, C., and D. J. Read, "Linear rheology of linear polydisperse polymers," see https://github.com/chinmaydaslds/LP2R (2022).